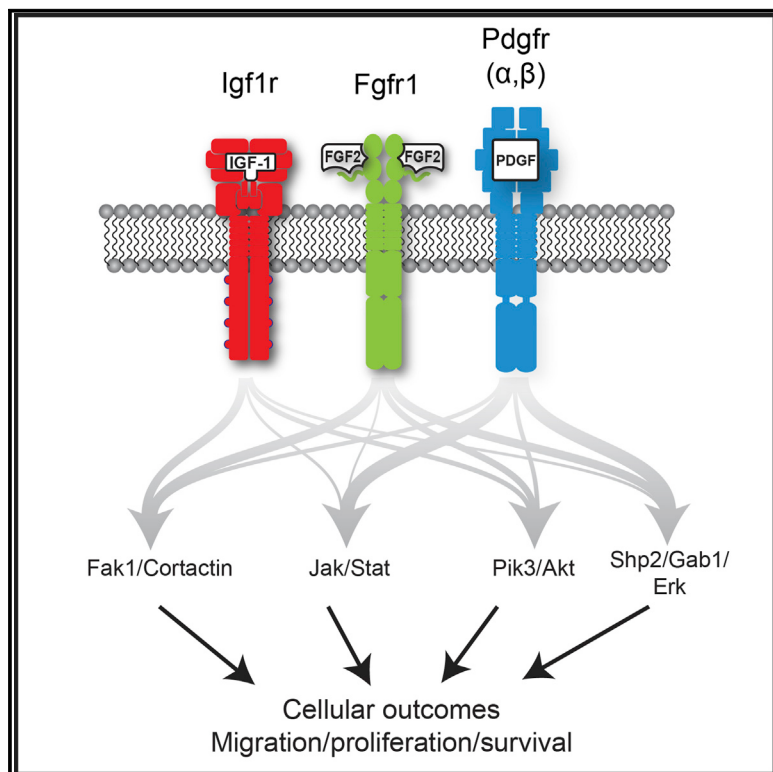


## Large-Scale Phosphoproteomics Reveals Shp-2 Phosphatase-Dependent Regulators of Pdgf Receptor Signaling

### Graphical Abstract



### Authors

Tanveer S. Bath, Moreno Papetti, Anamarija Pfeiffer, Maxim A.X. Tollenaere, Chiara Francavilla, Jesper V. Olsen

### Correspondence

chiara.francavilla@manchester.ac.uk  
(C.F.),  
jesper.olsen@cpr.ku.dk (J.V.O.)

### In Brief

Bath et al. use mass spectrometry-based phosphoproteomics to analyze receptor tyrosine kinase signaling activated by different ligands, identifying hundreds of differentially regulated phosphotyrosine sites. Tyrosine phosphatase Shp-2 regulates global tyrosine phosphorylation in a Pdgf-receptor-dependent manner, affecting cellular outcomes.

### Highlights

- Study of global phosphoproteome response after activation of different RTKs
- Shp-2 is highly phosphorylated upon Pdgf, but not Fgf-2, stimulation
- Application of an allosteric Shp-2 inhibitor reveals phosphotyrosine targets of Shp-2
- Pdgf-receptor-dependent cell migration is controlled by Shp-2

### Data and Software Availability

PXD005803



# Large-Scale Phosphoproteomics Reveals Shp-2 Phosphatase-Dependent Regulators of Pdgf Receptor Signaling

Tanveer S. Batth,<sup>1,4</sup> Moreno Papetti,<sup>1,4</sup> Anamarija Pfeiffer,<sup>1</sup> Maxim A.X. Tollenaere,<sup>2</sup> Chiara Francavilla,<sup>1,3,\*</sup> and Jesper V. Olsen<sup>1,5,\*</sup>

<sup>1</sup>Proteomics Program, Novo Nordisk Foundation Center for Protein Research, Faculty of Health and Medical Science, University of Copenhagen, Blegdamsvej 3B, 2200 Copenhagen, Denmark

<sup>2</sup>Cellular Stress Signaling Group, Department of Cellular and Molecular Medicine, Center for Healthy Aging, University of Copenhagen, 2200 Copenhagen, Denmark

<sup>3</sup>School of Biological Sciences, FBMH, University of Manchester, Oxford Road, Manchester M13 9PT, UK

<sup>4</sup>These authors contributed equally

<sup>5</sup>Lead Contact

\*Correspondence: chiara.francavilla@manchester.ac.uk (C.F.), jesper.olsen@cpr.ku.dk (J.V.O.)

<https://doi.org/10.1016/j.celrep.2018.02.038>

## SUMMARY

Despite its low cellular abundance, phosphotyrosine (pTyr) regulates numerous cell signaling pathways in health and disease. We applied comprehensive phosphoproteomics to unravel differential regulators of receptor tyrosine kinase (RTK)-initiated signaling networks upon activation by Pdgf- $\beta\beta$ , Fgf-2, or Igf-1 and identified more than 40,000 phosphorylation sites, including many phosphotyrosine sites without additional enrichment. The analysis revealed RTK-specific regulation of hundreds of pTyr sites on key signaling molecules. We found the tyrosine phosphatase Shp-2 to be the master regulator of Pdgfr pTyr signaling. Application of a recently introduced allosteric Shp-2 inhibitor revealed global regulation of the Pdgf-dependent tyrosine phosphoproteome, which significantly impaired cell migration. In addition, we present a list of hundreds of Shp-2-dependent targets and putative substrates, including Ras1 and Cortactin with increased pTyr and Gab1 and Erk1/2 with decreased pTyr. Our study demonstrates that large-scale quantitative phosphoproteomics can precisely dissect tightly regulated kinase-phosphatase signaling networks.

## INTRODUCTION

With advances in proteomic technologies, it is possible to comprehensively analyze human cell proteomes on par with next-generation genomic sequencing (Bekker-Jensen et al., 2017; Kim et al., 2014). However, routine analysis of post-translational modifications (PTMs) remains challenging due to their generally low cellular abundance and dynamic nature. Above all, site-specific protein phosphorylation on serine, threonine, and tyrosine residues is of great importance in eukaryotic cells due to their crucial role in rapidly regulating essentially all intracellular signaling networks

(Olsen et al., 2006). Protein phosphorylation is tightly regulated in healthy cells by the opposing action of protein kinases and phosphatases, which are the enzymes that write and erase this modification, respectively (Ubersax and Ferrell, 2007). Phosphotyrosine (pTyr) in particular remains elusive in its detection due to its highly transient and regulatory nature, which leads to overall lower phosphorylation stoichiometry and cellular abundance relative to its phosphoserine (pSer) and phosphothreonine (pThr) counterparts, which are readily observed in global phosphoproteomic experiments (Sharma et al., 2014). As a result, many large-scale cell signaling studies may inadvertently omit pTyr analysis and thereby overlook a vital layer of information regulating cell signaling and outcome. Obtaining greater molecular understanding of pTyr-driven signaling (alongside pSer and pThr) is the foundation for understanding signaling networks such as those initiated by receptor tyrosine kinases (RTKs), which are able to receive extracellular signals and relay them inside the cell plasma membrane, ultimately affecting cell fate, such as survival, differentiation, proliferation, and migration (Lemmon and Schlessinger, 2010). Consequently, RTKs and proteins involved in their downstream signaling tend to be highly oncogenic and thus the foremost drug targets in various cancers (Koytiger et al., 2013).

To address this challenge, we developed a streamlined phosphoproteomic framework based on high-pH reversed-phase chromatography (Wang et al., 2011) with automatic fraction concatenation followed by sensitive liquid chromatography-tandem mass spectrometry (LC-MS/MS) analysis. This enabled global detection of pSer, pThr, and pTyr sites in a single analysis without the need for phosphotyrosine-specific antibody pull-downs. By primarily using phosphotyrosine site regulation as the proxy of early signaling events, the initial analysis allowed us to observe distinct activation of numerous signaling pathways with RTK ligand treatment. We found platelet-derived growth factor receptor (Pdgfr) ( $\alpha$  and  $\beta$  subunits) to be a potent activator of most downstream signaling pathways. We observed that Shp-2 acts as a master regulator of the mitogen-activated protein kinase/extracellular-regulated kinase (Mapk/Erk) pathway for Pdgfr, and through the application of an allosteric Shp-2 phosphatase inhibitor, in combination with quantitative



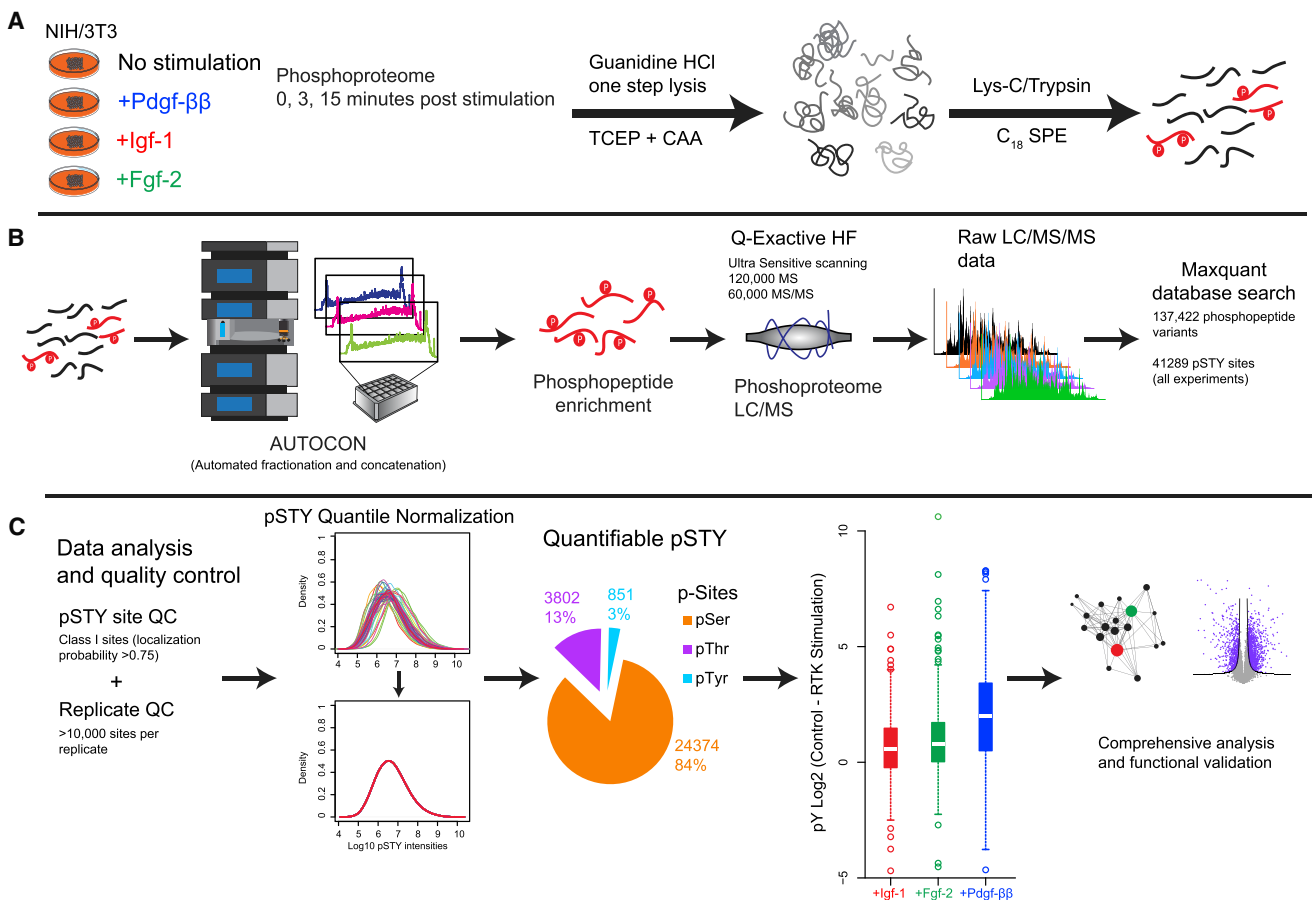


**Figure 1. Experimental Design and Phosphoproteomic Workflow Allows Comprehensive Analysis of Phosphorylation Sites**

(A) NIH/3T3 cells were stimulated with three RTK ligands (Pdgf- $\beta\beta$ , Fgf-2, and Igf-1) at the indicated time points, followed by rapid lysis, protein extraction, and digestion into tryptic peptides (see Materials and Methods).

(B) Peptides were automatically peptide fractionated and concatenated using high-pH reversed-phase chromatography in batch mode (AUTOCON) (Movie S1). For phosphoproteomic analysis, fractionated peptides were enriched using TiO<sub>2</sub> metal oxide affinity enrichment. Resulting phosphopeptides were analyzed by LC-MS/MS, where a highly sensitive MS scanning method was used and database search analysis of raw data was performed using MaxQuant as described in Materials and Methods.

(C) Overview of data analysis is shown; details are given in Materials and Methods. For phosphoproteomics, data were filtered and normalized to ensure fair comparison across all samples. The resulting phosphoproteome datasets resulted in a large number of phosphosites, including phosphotyrosine (pTyr) sites. Cells stimulated with Pdgf- $\beta\beta$  showed the largest number of regulated pTyr sites (which were also measured in control, non-stimulated samples). See also Figures S1 and S2 and Table S1.

phosphoproteomics, our analysis revealed global rewiring of the tyrosine phosphoproteome in a Pdgf- $\beta\beta$ -dependent manner. This dataset also provides a list of putative Shp-2 substrates, which include proteins regulating downstream RTK signaling pathways important for cellular outcomes such as proliferation and migration. Collectively, our investigation may increase our mechanistic insight into RTK signal propagation and phosphatase action.

## RESULTS

### Antibody-Free Screen Enables Unbiased In-Depth Identification of Phosphorylation Sites

We employed an optimized phosphoproteomic workflow based on label-free quantitation to unravel regulators of downstream RTK signaling networks mediated by three activated RTKs. We

investigated the global phosphosignaling response initiated by three RTKs in mice fibroblast NIH/3T3 cells after stimulation with their respective canonical ligands: platelet-derived growth factor beta receptor (Pdgf- $\beta\beta$  ligand), fibroblast growth factor receptor 1 (Fgf-2 ligand), and insulin-like growth factor 1 receptor (Igf-1 ligand), which were selected due to their abundance (Figure S1A). Their ligands induced a downstream phosphorylation response, evidenced by the activation and phosphorylation of Mapk/Erk (Figure S1B). We performed time-resolved quantitative phosphoproteomics to study the dynamic processes underlying the activation of RTK signal transduction. Samples were collected after 3 and 15 min of ligand stimulation, followed by efficient lysis and protein extraction, cysteine reduction, and alkylation in one step as previously reported (Figure 1A) (Jerie-Christensen et al., 2016; Poulsen et al., 2013).

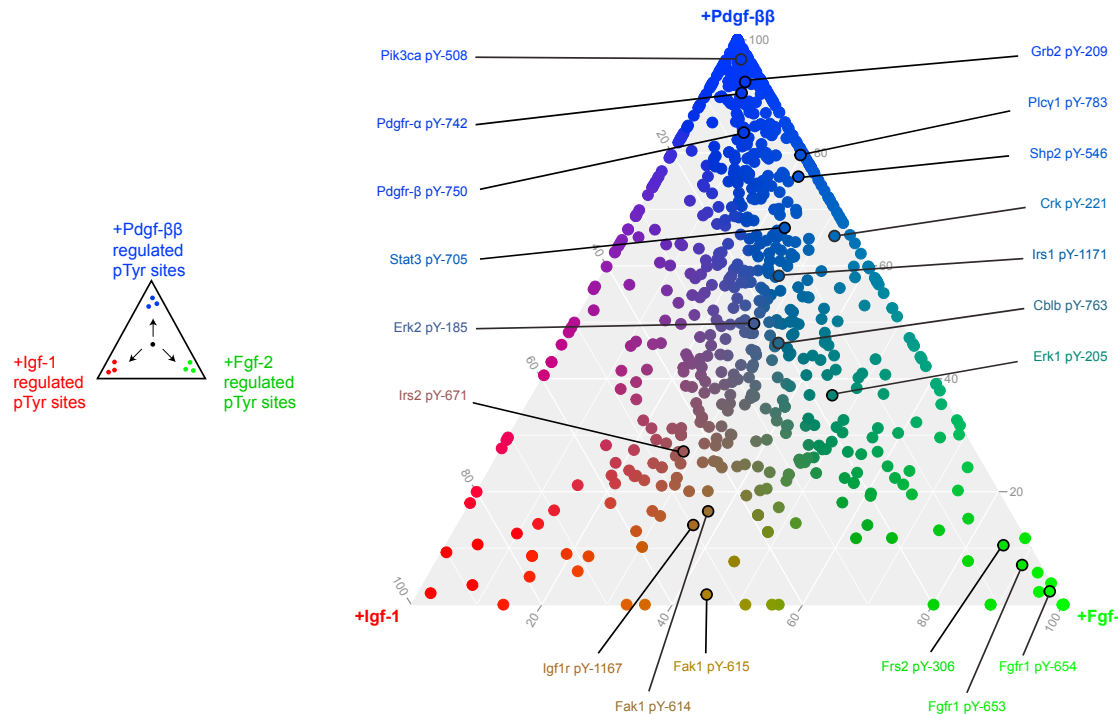


**Figure 2. Phosphoproteomic Analysis Discriminates Ligand-Induced Phosphorylation of Tyrosine Sites**

Tyrosine site phosphorylation intensities are visualized in a ternary plot to highlight the differential phosphorylation patterns induced upon Pdgf- $\beta\beta$ , Fgf-2, and Igf-1 stimulation. Each dot represents one unique pTyr site. Both color coding and mapping are based on the fractional intensities observed for each pTyr site upon the different ligand stimulations. A maximum intensity between 3 and 15 min was used for individual sites. Corners indicate pTyr sites specifically responsive upon Pdgf- $\beta\beta$ , Fgf-2, or Igf-1 stimulation. Tyrosine sites plotted in the center are equally phosphorylated by the three ligands. See also Figure S3 and Table S1.

We have previously demonstrated an efficient strategy for offline fractionation of phosphopeptides based on high-pH fractionation, which enabled us to identify a large number of tyrosine-phosphorylated peptides, similar to what is typically observed with the extensive use of pan-anti-pTyr antibodies (Bath et al., 2014). To establish a streamlined and comprehensive phosphoproteomic workflow, we automated the offline fractionation and concatenation (AUTOCON) steps before mass spectrometry (MS) analysis (Movie S1), which allowed us to process samples in batch mode and increase our throughput and reproducibility (Figure 1B). The phosphoproteomic workflow enabled the identification of 41,289 phosphorylation sites covering more than 7,000 phosphoproteins. We applied a strict quality filter. The resulting phosphosite intensities covered a large dynamic range, more than 6 orders of magnitude in each experiment, and 29,027 phosphorylation sites were quantifiable across conditions (Table S1). Analysis of the phosphorylated amino acid distribution showed that 84% of phosphorylation sites were on serine, whereas the 13% were threonine phosphorylation sites (Figure 1C). In addition, 851 (3%) of the total quantifiable phosphorylation sites belonged to tyrosine-containing peptides (Figure 1C), pinpointing a major strength of our workflow in achieving high pTyr coverage without pretreating cells with pervanadate.

Phosphotyrosine sites were roughly 2-fold lower in abundance compared to pSer and pThr (Figure S2A), which underscores the general challenges in detecting them by MS. Our workflow led to

an efficient accumulation of phosphotyrosine-containing peptides over the 12 high-pH fractions (Figure S2B), resulting in the identification of pTyr sites on more than 500 proteins enriched for RTK signaling, kinase activity, and protein binding and inclined to be localized at the plasma membrane and cytoplasm (Figure S2C). These data demonstrate the streamlined and comprehensive phosphoproteomic workflow encompassing serine, threonine, and pTyr.

#### Global Analysis of pTyr Sites

We analyzed the ligand-induced distribution of the quantified pTyr sites to gain insights into pTyr signaling upon differential RTK stimulation. Specifically, the proportional response in the pTyr site intensities (ternary plot) (Figure 2) distinguished the stimulating condition under which the sites are distributed relative to one another. Activated Pdgfr was the most potent regulator of pTyr sites when compared to Fgfr1 and Igf1r, as shown by a large cluster of pTyr sites at the top of the ternary plot, indicating higher relative response. Density estimation of all phosphorylation sites under the three RTK stimulation conditions indicated that this phenomenon was not global and was limited only to pTyr, because similar distributions were not observed for pSer and pThr sites (Figure S3). We found 21 pTyr sites on the cytoplasmic tail near the C terminus of Pdgfr- $\alpha$  (11) and Pdgfr- $\beta$  (10) subunits (Heldin and Lennartsson, 2013) to be exclusively detected upon Pdgf- $\beta\beta$  stimulation. In addition, we

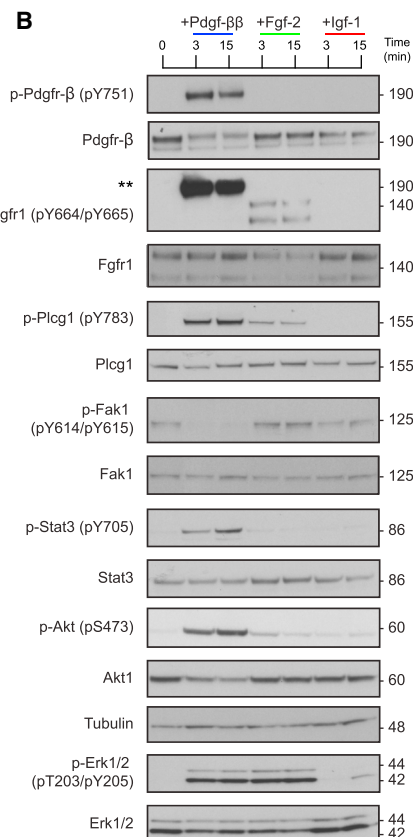
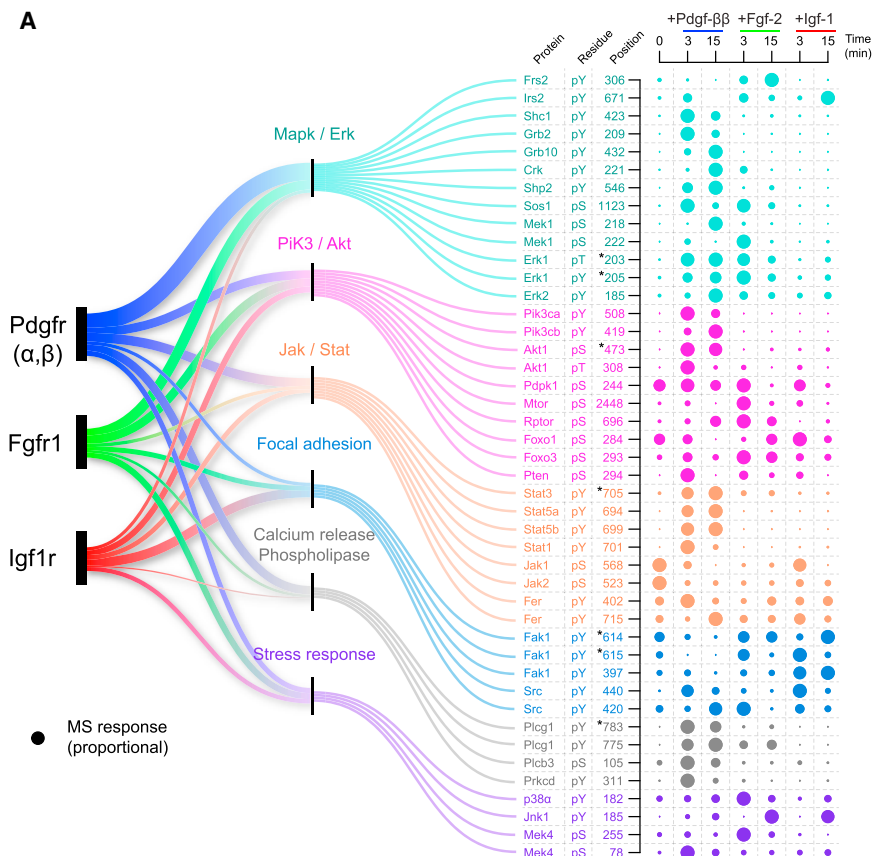


**Figure 3. Phosphoproteomic Analysis Reveals Differential Ligand-Induced Activation of Signaling Pathways**

(A) Dynamic profiles of site phosphorylation on proteins involved in different signaling pathways upon Pdgf- $\beta\beta$ , Fgf-2, and Igf-1 stimulation are shown. The size of each dot is the mean of the site phosphorylation intensities among replicates, which were identified in each of the seven conditions. Bigger correlates with a strong induction of phosphorylation for the indicated site and condition. Relative maximum intensity values for each site were used to proportionally normalize the global site phosphorylation dynamic profile. Minimum values were set to 0.01 (on a scale to 1) for representative purposes.

(B) Lysates from NIH/3T3 cells stimulated with Pdgf- $\beta\beta$ , Fgf-2, and Igf-1 for the indicated time points were immunoblotted as indicated to validate the differential dynamic profile. Tubulin was used as loading control.

\*Confirmed by western blot, \*\*antibody cross-reaction for the activated form of Pdgfr- $\beta$  as indicated by the manufacturer. See also Figure S4 and Table S1.

found six pTyr sites on Fgfr1 and fibroblast growth factor receptor 2 (Fgfr2) when stimulated with Fgf-2 (Figure 2; Table S1) (Furdui et al., 2006). Sites on canonical adaptor molecules such as Grb2 (pY209), Frs2 (pY306), and Irs2 (pY671) were also identified, indicating their preferential binding to activated Pdgfr, Fgfr1, and Igf1r, respectively (Figure 2). The analysis demonstrated the sensitivity of our workflow for screening pTyr sites without the need for pan-anti-pTyr antibody-based enrichment and comparable to state-of-the-art, antibody-based, phosphotyrosine-focused studies (Abe et al., 2017). The number of tyrosine sites reported in this study were roughly 6-fold higher than those reported with the EasyPhos method, which was used to study insulin signaling (another RTK) *in vivo* over several time points (Humphrey et al., 2015).

#### Phosphorylation Site Dynamics Reveal Preferentially Activated Signaling Pathways

The distinct activation of pTyr sites upon ligand stimulation suggests that the response initiated by each ligand-RTK pair

differentially regulate downstream signaling pathways (Franca-villa et al., 2016). We visualized their temporal changes as quantitative dot blots (Figure 3A) and validated our results by western blot analysis and quantification (Figure 3B; Figure S4). We found Pdgf- $\beta\beta$  and Fgf-2 stimulation induced phosphorylation of the activation loop residues pT203 and pY205 on Mapk/Erk1 (Figure 3). However, we observed that Pdgf- $\beta\beta$  exclusively activated Pik3/Akt (i.e., Pik3ca pY508 and Akt1 pS473), as well as Jak/Stat (i.e., Stat3 pY705) and Plc- $\gamma$  (i.e., Plcg1 pY783) pathways. Conversely, Fgf-2-treated cells pinpointed a preferential phosphorylation of Y614 and Y615 on focal adhesion kinase 1 (Ptob2 or Fak1) (Figure 3B). Surprisingly, Pdgf- $\beta\beta$ -stimulated cells displayed a reduction in the basal level of phosphorylation of Y614 and Y615 on Fak1 at both time points despite the relatively high pTyr response seen upon Pdgf- $\beta\beta$  stimulation. Because Igf-1 stimulation did not significantly induce activation of major signaling pathways, the remainder of this study was focused on the comparative analysis of the signaling responses mediated by Pdgfr and Fgfr1 activation. Collectively, these data support

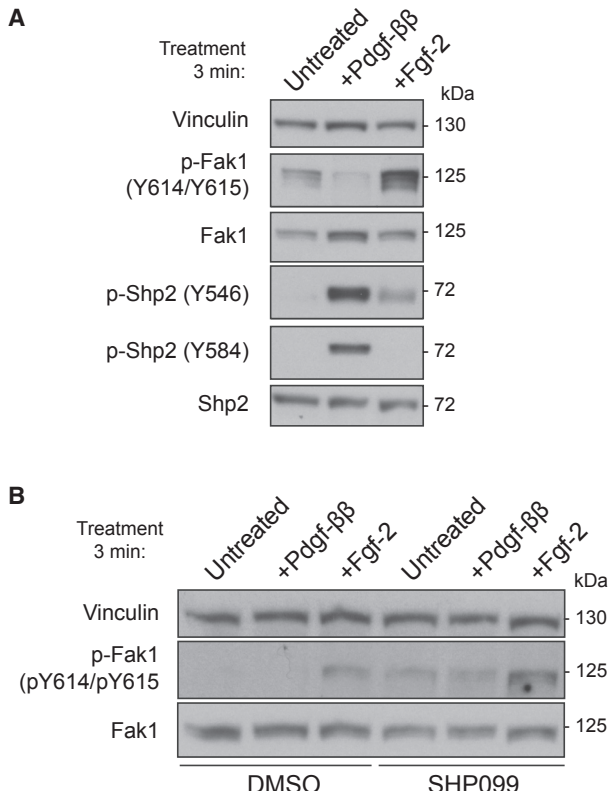


**Figure 4. Pdgf- $\beta\beta$ -Induced Activation of Shp-2 Affects Y614 and Y615 Phosphorylation on Fak1**

(A) Lysates from cells stimulated with Pdgf- $\beta\beta$ , Fgf-2, and Igf-1 for 3 min were immunoblotted as indicated. Bands related to Fak1 phosphorylation are shown after a longer exposure to emphasize the differences across the conditions.

(B) Lysates from cells stimulated with Pdgf- $\beta\beta$ , Fgf-2, and Igf-1 for 3 min were analyzed by immunoblotting with the designated antibodies. When indicated, cells were treated with SHP099 for 30 min before ligand stimulation.

Vinculin was used as loading control. SHP099, Shp-2 inhibitor. See also Figure S5.

the comprehensive phosphorylation workflow to investigate dynamic RTK signaling pathways.

#### Fak1 Dephosphorylation Correlates with Pdgfr-Dependent Shp-2 Activation

We hypothesized the presence of a Pdgf- $\beta\beta$ -dependent regulatory mechanism leading to Y614 and Y615 dephosphorylation on Fak1. We speculated that activated tyrosine phosphatases might play a role in mediating this and confirmed the possibility with global inhibition of tyrosine phosphatase activity with pervanadate (Figure S5A). Thus, we examined phosphatases exclusively tyrosine phosphorylated upon Pdgfr activation. We found protein tyrosine phosphate non-receptor type 11 (Shp-2 encoded by *PTPN11*) to be a putative candidate, because it displayed pronounced (a more than 60-fold increase) pTyr at positions Y546 and Y584, sites known to positively regulate Shp-2 enzymatic activity (Figures 3A and 4A; Table S1) (Zhang et al., 2015). We reasoned that Pdgfr-mediated activation of

Shp-2 might be responsible for Y614 and Y615 dephosphorylation on Fak1 (Mañes et al., 1999). We tested the impact of Shp-2 inhibition on Fak1 Y614 and Y615 dephosphorylation by a newly developed allosteric Shp-2 inhibitor SHP099 (Chen et al., 2016) and observed that Shp-2 inhibition in Pdgf- $\beta\beta$ -treated cells led to increased Y614 and Y615 phosphorylation on Fak1 (Figure 4B). Although an increase of phosphorylation on Fak1 was also observed upon Fgf-2 treatment in the presence of the inhibitor, it was less pronounced relative to Pdgf- $\beta\beta$  stimulation (with SHP099), which inverted the phosphorylation dynamics on these two Fak1 pTyr sites. The results indicate that Shp-2 is an active player in Pdgfr signaling and directly affects Fak1 phosphorylation.

#### Shp-2 Regulates the Global Pdgfr Phosphoproteome Landscape

We characterized the overall impact of Shp-2 activation in Pdgfr-mediated phosphosignaling response with a stable isotope labeling by amino acids in cell culture (SILAC)-based approach, in combination with phosphotyrosine peptide pull-down (Figure 5; Figure S6A) (Ong et al., 2002). Our findings revealed global changes in phosphorylation upon Pdgfr activation in Shp-2-inhibited cells (Figure S6B). Approximately 20% (1,428) of 6,884 quantified phosphorylation sites were statistically regulated more than 2-fold in the presence of SHP099 with Pdgf- $\beta\beta$  stimulation (based on Student's t test,  $p < 0.05$ ) (Table S2). Relative to serine and threonine phosphorylation sites, pTyr was mostly upregulated with Pdgf- $\beta\beta$  stimulation, alongside Shp-2 inhibitor (Figures S6B–S6E). Phosphotyrosine sites that were  $\geq 2$ -fold upregulated ( $p < 0.05$  based on Student's t test) upon Pdgf- $\beta\beta$  stimulation in the presence of SHP099 were deemed Shp-2-putative substrates (Table S2).

Our results revealed the negative regulation of Fak signaling (pY614/615) by Shp-2/Pdgfr was reversed in the presence of SHP099. Furthermore, pY421 on cortactin (Ctnn), a known important substrate of Fak signaling that is suggested to modulate cytoskeletal organization and cell motility, displayed dramatic increase in phosphorylation upon Pdgf- $\beta\beta$  stimulation when cotreated with SHP099 (Figure S7A; Table S2) (Tomar et al., 2012). We confirmed the dynamics of this key site on Ctnn by using a site-specific antibody for pY421, which was abolished in the presence of Fak1 inhibitor PF-562271 (Figure 5B). In addition, Shp-2 and Fak1 were found to be constitutively associated and recruited to the Pdgfr signaling complex upon Pdgf- $\beta\beta$  stimulation (Figures S7B and S7C).

Moreover, the results confirmed the specificity of Shp-2 inhibitor (SHP099) in inhibiting the Mapk/Erk pathway activation via significant downregulation of phospho-Erk1/2 activation sites pY185/205 (Chen et al., 2016). As a consequence, we identified many of the downregulated pSer sites that are predicted Erk1/2 substrates (Table S2). However, other signaling pathways were largely unaffected by Shp-2 inhibition, as determined by phosphorylation of prominent activation sites on Akt (pS473) and Stat (pY705), as well as pTyr sites on Plcg1 and Pik3c, which had unchanged or increased phosphorylation (Table S2). Our dataset demonstrates global upregulation of most phosphotyrosine signaling pathways by Shp-2 inhibition but accompanied by deactivation of the Mapk/Erk signaling cascade.

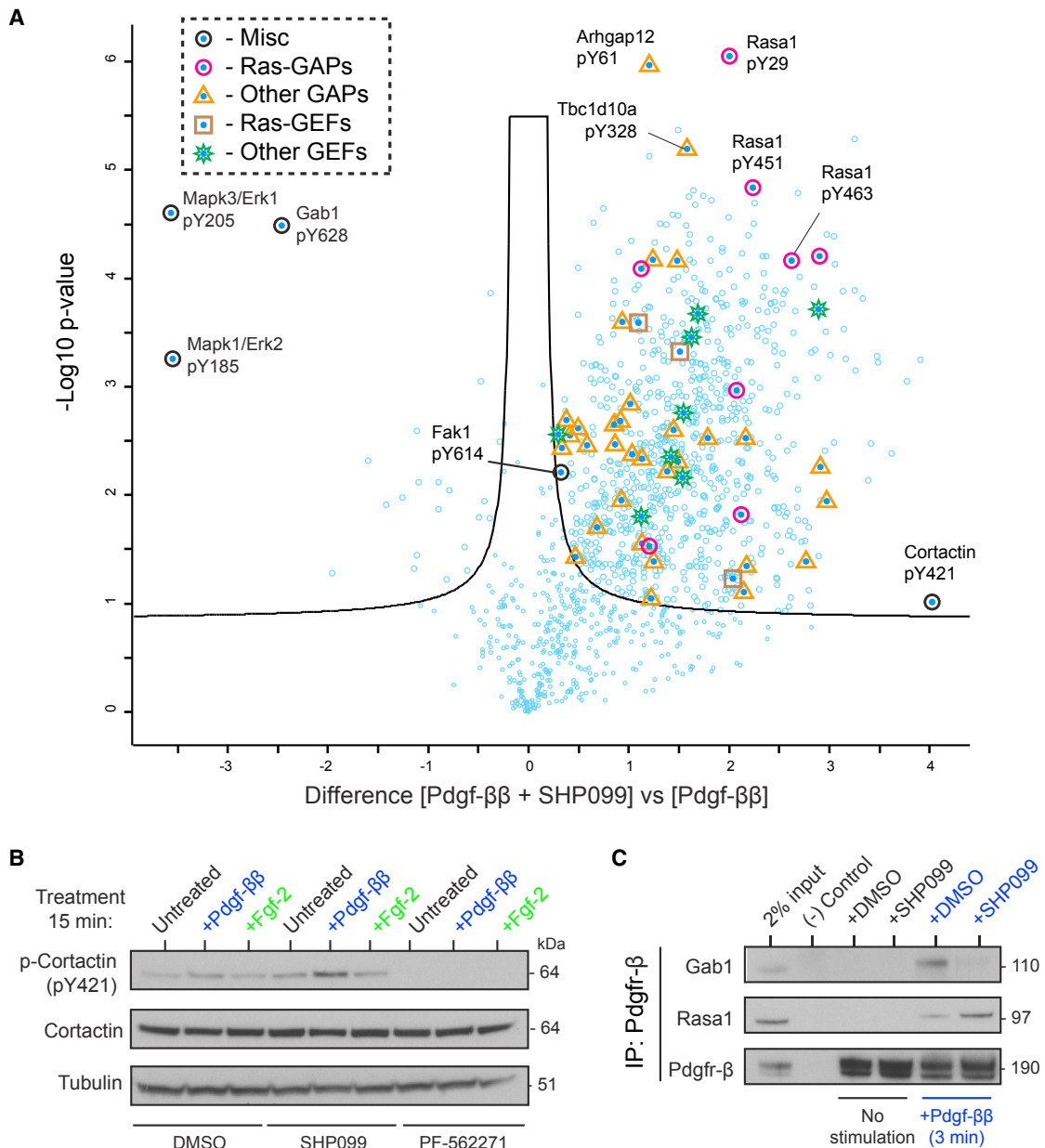


**Figure 5. Shp-2 Inhibition Induces Large Changes in Pdgfr-Induced pTyr, Affecting Interaction and Signaling**

(A) Volcano plot of SILAC phosphotyrosine site (class I) ratios after 15 min of Pdgf- $\beta\beta$  stimulation with and without Shp-2 inhibitor SHP099 at a false discovery rate (FDR) of 0.05 and small positive constant to minimize the coefficient of variation (S0) at 0.1 (see Materials and Methods for SILAC data analysis). Phosphotyrosine sites on the right side of the volcano plot were significantly upregulated when SHP099 is used alongside Pdgf- $\beta\beta$  stimulation, and sites were downregulated on the left side. Regulated sites on proteins containing different GAP and guanine nucleotide exchange factor (GEF) domains are highlighted.

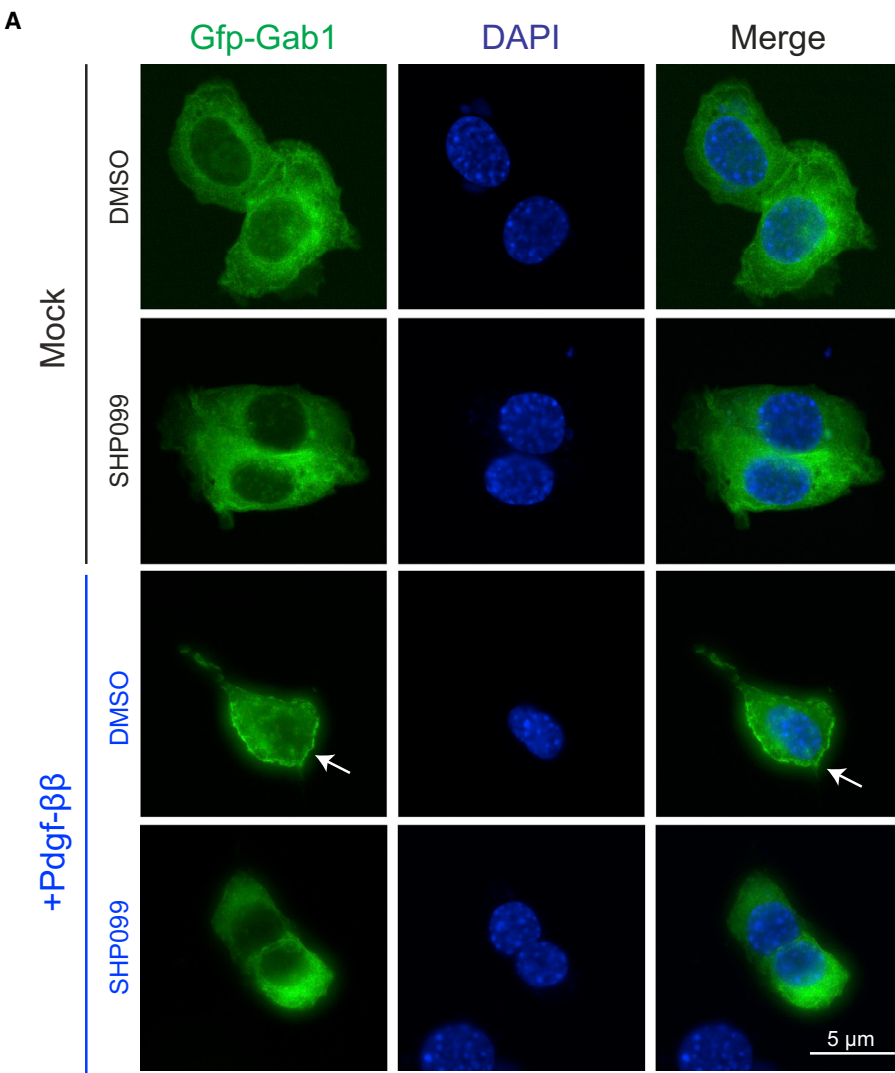
(B) Indirect regulation of cortactin phosphorylation at pY421 (target of Fak1) is confirmed via Fak1 inhibition with inhibitor PF-562271.

(C) Interaction of Gab1 and Rasa1 with Pdgfr- $\beta$  via immunoprecipitation shows decreased receptor-adaptor interaction of Gab1 with Shp-2 inhibition when Pdgfr is activated with Pdgf- $\beta\beta$  stimulation. The opposite trend is observed for Rasa1, where an increase in interaction of these two proteins is observed. See also Figures S6 and S7 and Table S2.

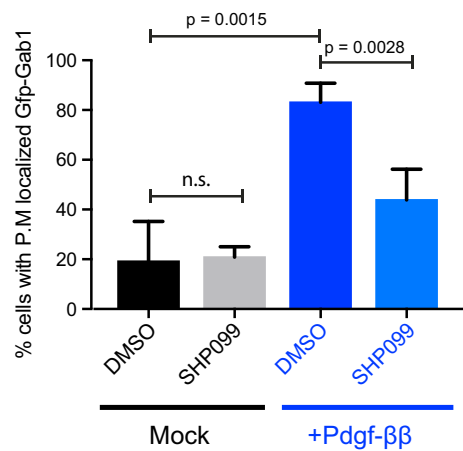
### Shp-2 Regulates the Interaction of Pdgfr with Signaling Proteins

Some of the most significantly upregulated pTyr sites with Shp-2 inhibition, alongside Pdgf- $\beta\beta$  stimulation, were found on proteins harboring guanosine triphosphatase (GTPase)-activating protein

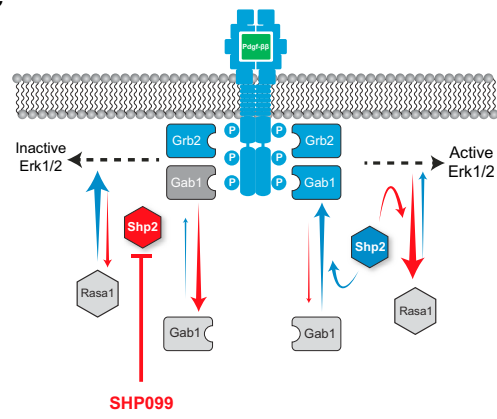
(GAP) domains (Figure 5A). We found significantly upregulated pTyr sites on GAP proteins spanning several GTPase families, such as Rasa1, Arhgap12, and Tbc1d10a (Figure 5A; Table S2). Increased levels of Rasa1, a Ras-specific GTPase, were observed to coimmunoprecipitate with Pdgfr upon Shp-2 inhibition and



**B** Gfp-Gab1 plasma membrane localization



**C**



(legend on next page)

Pdgf- $\beta\beta$  stimulation (Figure 5C). pTyr on the crucial adaptor protein Grb2-associated binder 1 (Gab1) at pY628 was significantly downregulated, alongside markers of Erk/Mapk pathway activation (via phospho-Erk1/2 sites pY185/205) in the presence of Shp-2 inhibitor. Gab1-induced Erk activation after Met receptor activation has previously been shown to depend on Shp-2 activity (Maroun et al., 2003). Therefore, we hypothesized that this could be equivalent in Pdgfr-activated cells. We found Gab1 to significantly decrease its interaction with Pdgfr in the presence of Shp-2 inhibition (Figure 5C). Because Gab1 is known to be targeted to the plasma membrane upon RTK stimulation (Chang et al., 2015), we observed an accumulation of Gab1 to the plasma membrane upon Pdgf- $\beta\beta$  stimulation (Figure 6). However, there was a significant reduction of Gab1 recruitment to the cellular plasma membrane after Pdgf- $\beta\beta$  stimulation in the presence of SHP099 (Figure 6B). The results indicate dynamic Shp-2-dependent regulation of key proteins, leading to changes in protein localization and pathway activation (Figure 6C).

### Shp-2 Affects Ligand-Dependent Cellular Outcomes

We next sought to determine the impact of Pdgfr- and Fgfr1-mediated signaling on cellular outcomes. Pdgf- $\beta\beta$ -induced cell migration and proliferation were both affected by Shp-2 inhibition, whereas Fgf-2-induced cellular responses were not (Figure 7). Specifically, Shp-2 inhibition, alongside Pdgf- $\beta\beta$  costimulation, of cells significantly reduced the rate at which cells migrated, while this was not observed with Fgf-2 stimulation in the presence of inhibitor (Figures 7A and 7B). The opposite trend was observed for cell proliferation in cells coexposed to SHP099 and Pdgf- $\beta\beta$ , displaying slightly higher proliferation rates comparable to Fgf-2 treatment. Conversely, SHP099 treatment, in combination with Fgf-2 stimulation, failed to affect the proliferation rate significantly (Figure 7C). Collectively, the results indicate an active role for Shp-2 in dictating Pdgf- $\beta\beta$ -mediated cellular migration, but not Fgf-2-dependent signaling and cellular responses.

## DISCUSSION

Tight regulation of the interplay among multiple cell signaling networks activated by RTKs is necessary to ensure normal cellular function. Identifying signaling proteins and quantifying their phosphorylation status directly by phosphoproteomics is emerging as an alternative to indirect approaches based on inferring cellular signaling network rewiring via genomic and transcriptomic studies (Yaffe, 2013). In this work, we demonstrate proof-of-principle of detecting and quantifying phosphotyrosine-containing peptides simultaneously with pSer and pThr without additional affinity purification via cocktails of pan-anti-pTyr antibodies. This foundation proved to be essential in the

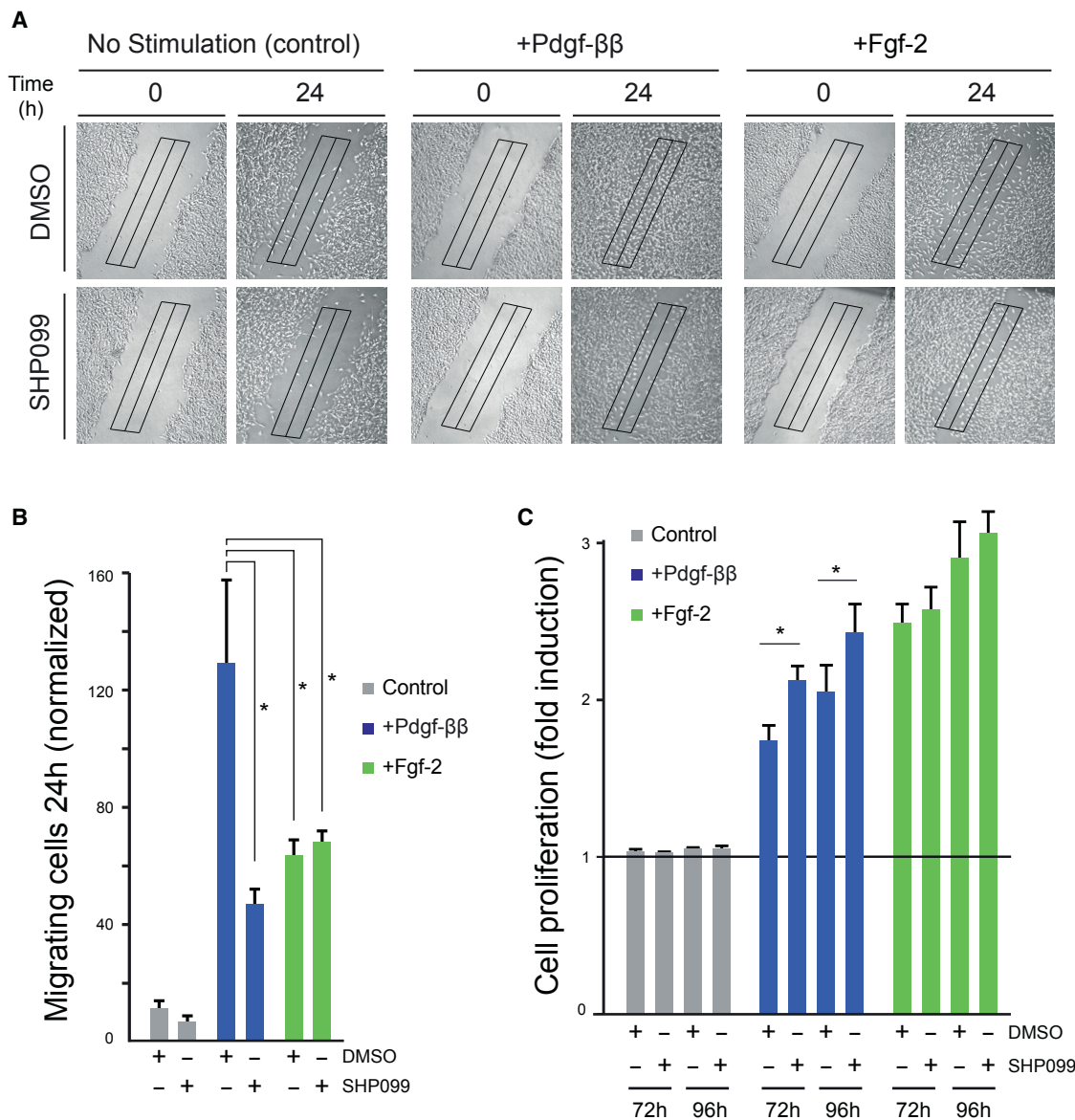
global investigation of endogenous RTK signaling and activation in murine fibroblast cells. The dataset will serve as a valuable resource for further follow-up of novel proteins and phosphorylation sites that may be involved in regulating downstream RTK response. Because Pdgfr is a crucial RTK implicated in numerous cancers and a prominent target for therapy, understanding its downstream signaling components could provide invaluable insight for treatment.

We conceptually demonstrated the potential of an antibody-free phosphoproteomic workflow by distinguishing the regulation of key downstream elements in Pdgfr signaling, such as Shp-2, Fak1, and Gab1, via pTyr. Although the relationships among these individual molecules have been well investigated as single- or two-component systems, our analysis pinpointed the interdependent regulation of each of these molecules simultaneously in an unbiased manner. The results highlight Shp-2 as a master regulator of downstream Pdgfr signaling while having modest to no influence on Fgfr signaling. Despite reduced cell migration upon Shp-2 inhibition, alongside Pdgfr activation, cell proliferation was surprisingly largely unaffected in our biological system. This could indicate different mechanisms of Mapk/Erk activation via activated Fgfr1 through distinct adaptor proteins such as Frs2. For instance, our results suggest that active Shp-2 is required for Gab1 recruitment to Pdgfr and the plasma membrane, which leads to full activation of the Erk/Mapk pathway. pTyr of Gab1 at pY628 has been suggested as a potential docking site for Shp-2 (Chan et al., 2010; Cunnick et al., 2001); however, it is possible that Shp-2 inhibition results in competitive Pdgfr interaction with an alternative protein superseding Gab1. It is conceivable that uncontrolled pTyr leads to the recruitment and localization of proteins and molecules that inhibit Erk1/2 activation. The significant increase in pTyr on several GAPs implies a crucial role in deactivating guanosine triphosphate (GTP)-bound Ras (active state), thus eliminating downstream activation of Erk via Ras/Raf/Mek. Unexpectedly, our results also indicate a potential role for GAPs, which have yet to be implicated with RTK signaling. Whether this results in reduced Gab1 pTyr and, as a consequence, reduced plasma membrane localization still needs to be determined. It is also plausible that additional molecular mechanisms and proteins could be involved in a synergistic or cumulative manner, leading to Mapk/Erk inhibition. Nonetheless, our dataset opens up the avenue for further examination of the role of several proteins that may regulate additional RTK signaling pathways in a similar manner and could serve as novel therapeutic targets.

The importance of phosphotyrosine signaling in health and disease is unquestionable, but global and unbiased tyrosine phosphoproteomic investigations have so far been limited due to its low cellular abundance. We demonstrated the benefits of

### Figure 6. Immunofluorescence Imaging of Gfp-Gab1 Shows Treatment-Dependent Cellular Localization

(A) Representative immunofluorescent cell images of Gfp-Gab1 cell nucleus with DAPI staining of NIH/3T3 cells under different treatment conditions. For imaging, cells were cooled to 4°C for 30 min before stimulation with Pdgf- $\beta\beta$ . (B) Quantitation of Gab1 localization was determined by manually counting the number of cells, which displayed Gfp-Gab1 membrane localization. Four biological replicates ( $n = 4$ ) performed on two separate days were used to determine statistical significance. Each biological replicate represents a different coverslip. Between 11 and 48 cells were counted for each coverslip. Error bars represent SD, and the p value was determined by unpaired two-tailed t test. (C) Schematic model of the role of Shp-2 in Pdgfr signaling is illustrated. Inhibition of Shp-2 results in increased localization of Rasa1 to Pdgfr (as indicated by arrows) and the reverse for Gab1.

**Figure 7. Shp-2 Is Involved in Pdgf- $\beta\beta$ -Dependent Cellular Responses**

(A) Cell migration upon ligand stimulation after 24 hr was detected by wound healing assay. Representative wound closure images of the scratch cross-sectional areas from three experiments are shown.

(B) Cell migration was calculated as described in Materials and Methods. Values are normalized to their respective 0 hr time point and presented as means  $\pm$  SEM of three independent experiments.

(C) Cell proliferation assay upon ligand stimulation after 72 and 96 hr. Black lines represent control cells. Results are expressed as fold induction (means  $\pm$  SEM) from three independent experiments.

SHP099, Shp-2 inhibitor. \*p < 0.05 (Student's two-tailed t test).

a global phosphoproteomic workflow for elucidating differential endogenous RTK signaling networks and expect similar workflows to be routinely applied directly toward analyzing signaling in tumor and cancer tissues. This provides opportunities to identify new biomarkers and drug candidates. As such, we hope that our datasets will serve as a beneficial foundation for further validation and mechanistic elucidation of several novel proteins that could be implicated in modulating downstream RTK signaling.

## EXPERIMENTAL PROCEDURES

### Reagents

The following commercial reagents were used: Fgf-2, Pdgf- $\beta\beta$ , and Igf-I (PeproTech); DMSO (Sigma-Aldrich); Shp-2 inhibitor SHP099 (Xcessbio); Fak1 inhibitor PF-562271 (Selleckchem); and Mek inhibitor U0126 (Cell Signaling Technology). Antibodies were as follows: rabbit anti-phospho-Fak (pY576/pY577); rabbit anti-Fak, rabbit anti-phospho-Akt (pS473); rabbit anti-Akt, mouse anti-phospho-Stat3 (pY705); rabbit anti-Stat3, rabbit

anti-phospho-Pdgfr- $\beta$  (pY751); rabbit anti-Pdgfr- $\beta$ , mouse anti-phospho-Fgrf1 (pY653/654); rabbit anti-phospho-Plcy1 (pY783); rabbit anti-phospho-Ctnn (pY421); rabbit anti-Ctnn, rabbit anti-Plcy1, rabbit anti-phospho-Shp-2 (pY542); rabbit anti-phospho-Shp-2 (pY580); rabbit anti-Shp-2, rabbit anti-Gab1, mouse anti-phospho-Erk1/2 (pT202/pY204); and rabbit anti-Erk1/2 (Cell Signaling Technology); rabbit anti-Erk1/2, mouse anti-vinculin, and mouse anti-tubulin (Sigma-Aldrich); rabbit anti-Fgrf1, mouse anti-Ras GAP (Santa Cruz Biotechnology); and mouse anti-Grb2 (BD Biosciences). Bead-conjugated antibodies for phosphotyrosine enrichment were mouse anti-phosphotyrosine (P-Tyr-100) and rabbit anti-phosphotyrosine (P-Tyr-1000) (Cell Signaling Technology).

#### Cell Culture and Ligand Stimulation

NIH/3T3 *Mus musculus* fibroblast adherent cell cultures were purchased from ATCC. Cells were cultured in DMEM (Gibco), 100 U/mL penicillin (Invitrogen), and 100  $\mu$ g/mL streptomycin (Invitrogen) and supplemented with 10% newborn calf serum (NBCS) (Gibco) at 37°C in a humidified incubator with 5% CO<sub>2</sub>. For the ligand stimulation experiment, cells were serum-starved overnight in serum-free medium. Cells were stimulated for the indicated time points with 100 ng/mL of Pdgf- $\beta$ , Fgf-2, or Igf-1. Ligands were replenished every 24 hr for long-term stimulation. All experiments were performed at 80% confluence on Nunc Petri dishes (245 or 150 mm) except for the wound healing scratch assay, for which 95% confluence was used. Experiments for cell-based assays were performed in either 24-well plates or 6-well plates. All cells were tested for mycoplasma with a PCR-based method every third week.

#### SILAC

NIH/3T3 cells were cultured in high-glucose DMEM (Biowest) lacking lysine and arginine supplemented with 10% dialyzed fetal bovine serum (Gibco), 2 mM L-glutamine (Gibco), 100 U/mL penicillin (Invitrogen), and 100  $\mu$ g/mL streptomycin (Invitrogen). Three cell populations were obtained: one labeled with natural variants of the amino acids: light label: Lys0, Arg0 (Sigma), the second labeled with medium variants of amino acids {L-[<sup>2</sup>H4]Lys (+4) and L-[<sup>13</sup>C6]Arg (+6)} (Lys<sup>4</sup>, Arg<sup>6</sup>), and the third labeled with heavy variants of the amino acids {L-[<sup>13</sup>C6, <sup>15</sup>N2]Lys (+8) and L-[<sup>13</sup>C6, <sup>15</sup>N4]Arg (+10)} (Lys<sub>8</sub>, Arg<sub>10</sub>). Medium and heavy variants of amino acids were purchased from Cambridge Isotope Laboratories. According to determined protein concentration via Bradford assay (Bio-Rad), proteins for each SILAC condition were mixed at 1:1:1 ratio.

#### Cell Lysis and Western Blots

For proteomic analysis, cells were quickly washed twice with cold 1× PBS after stimulation. Boiling lysis buffer (6 M guanidium hydrochloride and 25 mM Tris [pH 8]) containing 5 mM tris(2-carboxyethyl)phosphine (TCEP) and 5.5 mM chloroacetamide (CAA) was added to culture plates. Cells were then scraped and collected. Following collection, the samples were boiled at 99°C for 10 min, followed by sonication using a tip. Bradford assay (Bio-Rad, Hercules, CA, USA) was used to determine protein concentration. For biochemical assays, cells were washed twice with cold 1× PBS after stimulation. Cell extraction was performed in lysis buffer (50 mM Tris HCl [pH 7.6], 150 mM NaCl, and 1% Triton) supplemented with complete mini EDTA-free protease inhibitor (Roche) and 1 mM of sodium fluoride (NaF),  $\beta$ -glycerol phosphate, and sodium orthovanadate (Na<sub>3</sub>PO<sub>4</sub>). Following centrifugation at 13,000  $\times$  g for a least 20 min at 4°C, the protein concentration was determined using Bradford assay (Bio-Rad). When needed before stimulation, cells were preincubated for 30 min with 10  $\mu$ M U0126 and 10  $\mu$ M PF-562271 and for 1 hr with 10  $\mu$ M SHP099 inhibitor. Control cells were preincubated with DMSO alone. After sample collection, immunoblotting was performed as previously described (Francavilla et al., 2016). Quantification analysis was performed with ImageJ software, and images were processed by Photoshop and Illustrator software (CS6 version; Adobe). Each experiment was repeated at least three times and produced similar results.

#### Cell Proliferation Assay

Cells were seeded in triplicate on 24-well plates at 4  $\times$  10<sup>4</sup> cells/well, serum-starved overnight, and treated for either 72 or 96 hr with 100 ng/mL of Fgf-2,

Pdgf- $\beta$ , and Igf-1. When needed, cells were treated with 10  $\mu$ M SHP099 inhibitor and 10  $\mu$ M U0126 for the indicated time point, and control cells were treated with DMSO alone. Medium with fresh ligands and inhibitor was replenished every 24 hr. At each time point, viable cells were counted with trypan blue exclusion method, and the ratio to unstimulated cells at time 0 was determined for each time point as previously described (Francavilla et al., 2016). Values represent the means  $\pm$  SEM from at least three independent experiments performed in triplicate.

#### Wound Healing Scratch Assay

The migratory behavior of NIH/3T3 cells was evaluated using the scratch (wound healing) assay. Equal numbers of cells were seeded in triplicate on 6-well plates and allowed to reach confluence. Cells were then serum-starved overnight, and the wound was made by scratching a line across the bottom of the dish on a confluent cells monolayer. One wound per well was made using a sterile p-10 pipette tip spanning the well. Cells were rinsed gently with PBS and then treated for 24 hr with 100 ng/mL of Pdgf- $\beta$  or Fgf-2. When needed before stimulation, cells were preincubated with 10  $\mu$ M SHP099 inhibitor for 30 min. Control cells were preincubated with DMSO alone. Migration of cells was observed at premarked positions below the wells using a Leica DMI3000 inverted microscope at 5× magnification. Quantification was performed manually by counting the number of migrating cells within the scratch cross-sectional area. Values represent the means  $\pm$  SEM from at least three independent experiments performed in duplicate.

#### Immunoprecipitation

For pull-downs, stimulation was performed as described earlier and lysis was performed in the same manner as for biochemical assays. NIH/3T3 cell lysates (1 mg per condition) were precleared with anti-rabbit immunoglobulin G (IgG) (Sigma-Aldrich) supplemented with Protein G-Sepharose beads (Invitrogen) and inversion rotated for at least 2 hr at 4°C. After centrifugation at 1,000 relative centrifugal force (RCF) for 5 min, cleared samples were incubated with anti-Pdgfr- $\beta$  antibody overnight at 4°C (1:150 ratio). Protein G-Sepharose beads were added for 1 hr at 4°C, and the immunoprecipitated proteins were washed three times with ice-cold lysis buffer: once with 50 mM NaCl, once with 150 mM NaCl, and once with Milli-Q H<sub>2</sub>O. Proteins were eluted from beads by boiling in lithium dodecyl sulfate (LDS) sample buffer (Novex).

#### Immunofluorescence Imaging

For fluorescent microscopy, human Gab1 (transcript variant 1) was gateway cloned into the destination vector pcDNA4/TO/GFP. Cells were grown on coverslips and transfected with pcDNA4/TO/GFP-GAB1 using Fugene 6 (Promega) for 12 hr. After stimulation, cells were fixed in 4% formaldehyde and permeabilized with PBS containing 0.2% Triton X-100 for 5 min. Coverslips were mounted with Vectashield mounting medium (Vector Laboratories) containing the nuclear stain DAPI. Images were acquired with a Leica DMI6000B wide-field microscope (Leica Microsystems) equipped with an HC Plan-Apochromatic 63 $\times$ /1.4 oil immersion objective. Image acquisition and analysis were carried out with LAS X and ImageJ software.

#### Sample Prep for MS

Lys-C protease (Wako Chemicals, Richmond, VA, USA) at a 1:100 (w/w) ratio was used to digest proteins to peptides for 2 hr at 37°C. Samples were then diluted with 50 mM ammonium bicarbonate to <2 M guanidinium concentration, and trypsin was added at 1:50 (w/w) to generate tryptic peptides overnight at 37°C. Following digestion, samples were acidified with trifluoroacetic acid (TFA, 1% final) and centrifuged to remove debris. Peptides were then desalting on a C<sub>18</sub> sep-pak (Waters, Milford, MA, USA) and stored until further processing. Following elution with 50% acetonitrile, samples were concentrated using a SpeedVac.

#### Automated Concatenation and Fractionation of Tryptic Peptides

Ultimate 3000 ultra-high performance liquid chromatography (UHPLC) (Dionex, Sunnyvale, CA, USA), in conjunction with high-pH reversed-phase chromatography, was used to separate and fractionate tryptic peptides. Peptides were separated using a high-pH-compatible 250  $\times$  4.6 mm C<sub>18</sub> Waters BEH X-Bridge peptide separation technology (PST) 3.6  $\mu$ M or Phenomenex

Kinetex Evo 2.6  $\mu\text{M}$  (Torrance, CA USA) column with identical dimensions. Basic conditions were achieved by running buffer C (50 mM ammonium hydroxide) constantly at 10% (100  $\mu\text{L}/\text{min}$ , 5 mM ammonium hydroxide final). A 60 min fractionation and collection gradient was achieved using buffer A (Milli-Q H<sub>2</sub>O) and buffer B (acetonitrile), and fractions were collected at 1 min intervals and AUTOCON into 10 fractions in a 24-well plate ([Movie S1](#)). Running at a constant 1 mL/min, the gradient was increased from 5% to 25% buffer B in 50 min and further increased to 70% buffer B in 5 min, where it was held for another 5 min. At this point, the fraction collection was stopped. Each fraction sampled 6 points across the gradient, resulting in a 6-mL volume per fraction. 100  $\mu\text{L}$  were removed from each fraction for proteome analysis, 6 mL of 88% acetonitrile with 12% TFA was added to each fraction, and samples were stored.

#### TiO<sub>2</sub> Enrichment of Phosphopeptides

Each fraction was enriched with metal oxide affinity chromatography (MOAC) enrichment in batch mode by addition of titanium dioxide (TiO<sub>2</sub>) beads (GL Sciences, Japan) preincubated with 2,3-dihydroxybenzoic acid (DHB) and mixed for 20 min at room temperature. Fractions 1–5 and 6–10 were combined, and double-TiO<sub>2</sub> enrichment was performed to bring total number of fractions for phosphoproteome analysis per replicate to 12. TiO<sub>2</sub> beads were collected using centrifugation and washed on C<sub>8</sub> StageTips in a 96-well format. Phosphopeptides were eluted under basic conditions (5% ammonium hydroxide and 25% acetonitrile) and dried to remove residual acetonitrile. Phosphopeptides were then washed and loaded onto C<sub>18</sub> StageTips in a 96-well format, where they were stored until further analysis by LC-MS/MS.

#### Phosphotyrosine and pSer or pThr Peptide Enrichment

Phosphotyrosine-containing peptides were enriched using a 1:1 mixture of bead-conjugated anti-phosphotyrosine antibodies (PTM scan pY100 and pY1000, Cell Signaling Technology). One vial of each antibody was used for two samples. Bead-conjugated antibodies were washed 4× in 1 mL of PBS and resuspended in 3-(N-morpholino) propanesulfonic acid (MOPS) buffer. Peptides for phosphotyrosine enrichment were eluted from C<sub>18</sub> sep-pak with 40% and 60% acetonitrile (ACN). Eluted peptides were concentrated to a volume under 100  $\mu\text{L}$  using a vacuum concentrator and incubated at 4°C with 1.5 mL of immunoprecipitation buffer (50 mM MOPS [pH 7.2], 10 mM sodium phosphate, and 50 mM NaCl) overnight. Clarified peptides were separated by centrifugation at 10,000 RCF for 5 min at 4°C, and supernatants were transferred to a new tube. Antibodies were thereafter added to the samples and incubated for 2 hr at 4°C. The antibody-peptide complexes were washed 5 times with cold MOPS buffer, 2 times with 50 mM NaCl, 2 times with 150 mM NaCl, and 1 time with Milli-Q H<sub>2</sub>O. Supernatants of each wash were preserved for subsequent TiO<sub>2</sub> enrichment. Peptides were eluted from the antibodies using 300  $\mu\text{L}$  of 0.1% TFA twice and loaded on C<sub>18</sub> StageTips, where they were stored until further analysis by LC-MS/MS.

For phosphorylated serine and threonine (pST) enrichment, supernatant from pTyr enrichment was acidified using TFA and washed on C<sub>18</sub> sep-paks. Sep-paks were eluted as described earlier, and ACN and TFA were added to final concentrations of 80% and 5%, respectively. TiO<sub>2</sub> beads were added to the eluate, enriched for phosphopeptides, and prepared for LC-MS/MS analysis as described earlier. A second round of incubation was performed on the eluate, resulting in two samples for pST analysis.

#### Nano-liquid Chromatography and MS Analysis

Thermo Fisher Orbitrap HF (Bremen, Germany) mass spectrometer operating in positive mode coupled to Easy-nLC 1000 was used in the analysis of all samples. For phosphoproteomic analysis, all samples were analyzed with sensitive MS parameters. Spectra were acquired with survey MS scans at an Orbitrap resolution of 120,000 (full width at half maximum [FWHM]), from which the top 7 most abundant peaks were selected for higher-energy collisional dissociation (HCD) fragmentation and the resulting fragment spectra were collected at 60,000 MS/MS resolution. For proteome analysis, MS survey scan resolution of 60,000 was used and the HCD spectra were collected for the top 10 most abundant peaks at a resolution of 30,000. Peptides were separated in a 15-cm microbore column (75  $\mu\text{M}$  inner diameter) packed in-house with 1.9  $\mu\text{M}$  C<sub>18</sub> beads (Dr. Maisch, Germany) at 250 nL/min. Identical fast

gradient was used in the analysis of all samples. Buffer B (80% ACN and 0.1% formic acid) was increased from 5% to 35% in 55 min to 45% in 5 min. This was followed by a quick ramp up to 80% buffer B in 2 min. It was held there for additional 5 min before declining back down to 5% in 5 min, where it was held for an additional 5 min to re-equilibrate the column.

For single-shot analysis of SILAC pTyr and pST, sensitive scanning MS parameters were used as described earlier, except that the top 10 most abundant peaks were selected for HCD fragmentation. In addition, a longer gradient was used for single-shot analysis on a similar 15-cm column, consisting of an increase to 25% buffer B in 110 min followed by an increase to 40% buffer B in 25 min. After this, the column was increased to 80% buffer B in 5 min, where it was held for 5 min, followed by a ramp down to 5% buffer B for column re-equilibration.

#### LC-MS/MS Database Search

All files were processed together, and raw data were searched using MaxQuant v.1.5.3.33 with Andromeda search engine (<http://www.maxquant.org>) ([Cox and Mann, 2008](#)) against the *Mus musculus* uniprot database. The MS/MS spectra were searched with carbamidomethyl as a fixed modification on cysteine and variable modification oxidation on methionine, protein n-terminus acetylation, and phosphorylation on serine, threonine, and tyrosine, along with deamidation on asparagine and glutamine. A false discovery rate (FDR) of 1% was used at the peptide and protein level. Protein quantitation required minimum of two peptides without modifications.

#### Phosphoproteomic Analysis

Resulting identified phosphorylation sites (phospho STY/sites.txt table) from MaxQuant analysis were filtered only for those that were confidently localized (class I, localization probability  $\geq 0.75$ ). Replicates were retained only when >10,000 high-confident phosphorylation sites were present, resulting in a minimum of 5 replicates for each condition. Quantile normalization ([Figure 1C](#)) was used to normalize the phosphorylation data ([Bolstad et al., 2003](#)). A site was deemed quantifiable when it was observed a minimum of two times in at least one condition, resulting in >29,000 total quantifiable sites. The resulting quantile normalized sites were used for all analysis of phosphorylation data presented in this publication.

#### SILAC Analysis

SILAC phosphoproteome samples were analyzed with search parameters similar to those described earlier, with the addition of SILAC multiplicity indicating a triple SILAC setup. Resulting phosphorylation sites were analyzed in Perseus v.1.5.2. MaxQuant normalized ratios were used for quantitation. Phosphorylated serine, threonine, and tyrosine (pSTY) sites were expanded to differentiate multiple peptide phosphorylation states and filtered only for those that were confidently localized (class I, localization probability  $\geq 0.75$ ). Reverse and contaminant hits were removed from the analysis, and sites had to be observed for a minimum of 2 of 3 replicates in each of the 3 conditions to be considered for quantitation.

#### Proteome Analysis

Perseus v.1.5.2.6 was used for analysis of proteomics ([Tyanova et al., 2016](#)). For quantitative analysis of protein abundance changes, label-free quantitation (LFQ) values were employed ([Cox et al., 2014](#)), and intensity-based absolute quantification (iBAQ) analysis was used for relative expression analysis. Significant proteins were determined on log<sub>10</sub>-transformed LFQ values using a Student's t test.

#### DATA AND SOFTWARE AVAILABILITY

The accession number for the MS proteomic data reported in this paper is PRIDE: PXD005803 ([Vizcaino et al., 2014](#)).

#### SUPPLEMENTAL INFORMATION

Supplemental Information includes seven figures, two tables, and one movie and can be found with this article online at <https://doi.org/10.1016/j.celrep.2018.02.038>.

## ACKNOWLEDGMENTS

The authors thank Christian Kelstrup and Brian Weinert for helpful discussions and feedback. Work at The Novo Nordisk Foundation Center for Protein Research (CPR) is funded in part by a donation from the Novo Nordisk Foundation (grant NNF14CC0001). The applied proteomic technology developments were part of a project that has received funding from the European Union's Horizon 2020 research and innovation program (grant MSmed 686547). We would like to thank the PRO-MS Danish National Mass Spectrometry Platform for Functional Proteomics and the CPR Mass Spectrometry Platform for instrument support and assistance. C.F. was supported by a long-term EMBO fellowship and the Wellcome Trust (8107636/Z/15/Z). J.V.O. was supported by the Danish Cancer Society (R90-A5844 KBVU project grant) and Lundbeckfonden (R191-2015-703).

## AUTHOR CONTRIBUTIONS

J.V.O., C.F., and T.S.B. conceived and designed the project. T.S.B. developed the phosphoproteomic workflow and carried out the proteomic experiments. T.S.B. and J.V.O. carried out the initial data processing and analysis. M.P. and A.P. provided assistance in proteomic experiments and performed biological, molecular, and cellular biological experiments and follow-ups and contributed to manuscript writing. M.A.X.T. performed the immunofluorescence microscopy experiments and analysis. T.S.B. wrote the initial draft of the paper. M.P., J.V.O., C.F., and A.P. edited and contributed to the manuscript.

## DECLARATION OF INTERESTS

The authors declare no competing interests.

Received: October 16, 2017

Revised: January 2, 2018

Accepted: February 9, 2018

Published: March 6, 2018

## REFERENCES

- Abe, Y., Nagano, M., Tada, A., Adachi, J., and Tomonaga, T. (2017). Deep phosphotyrosine proteomics by optimization of phosphotyrosine enrichment and MS/MS parameters. *J. Proteome Res.* **16**, 1077–1086.
- Batth, T.S., Francavilla, C., and Olsen, J.V. (2014). Off-line high-pH reversed-phase fractionation for in-depth phosphoproteomics. *J. Proteome Res.* **13**, 6176–6186.
- Bekker-Jensen, D.B., Kelstrup, C.D., Batth, T.S., Larsen, S.C., Haldrup, C., Bramsen, J.B., Sørensen, K.D., Hoyer, S., Ørntoft, T.F., Andersen, C.L., et al. (2017). An optimized shotgun strategy for the rapid generation of comprehensive human proteomes. *Cell Syst.* **4**, 587–599.e4.
- Bolstad, B.M., Irizarry, R.A., Astrand, M., and Speed, T.P. (2003). A comparison of normalization methods for high density oligonucleotide array data based on variance and bias. *Bioinformatics* **19**, 185–193.
- Chan, P.-C., Sudhakar, J.N., Lai, C.-C., and Chen, H.-C. (2010). Differential phosphorylation of the docking protein Gab1 by c-Src and the hepatocyte growth factor receptor regulates different aspects of cell functions. *Oncogene* **29**, 698–710.
- Chang, C.-H., Chan, P.-C., Li, J.-R., Chen, C.-J., Shieh, J.-J., Fu, Y.-C., Chen, H.-C., and Wu, M.-J. (2015). Gab1 is essential for membrane translocation, activity and integrity of mTORCs after EGF stimulation in urothelial cell carcinoma. *Oncotarget* **6**, 1478–1489.
- Chen, Y.-N.P., LaMarche, M.J., Chan, H.M., Fekkes, P., Garcia-Fontanet, J., Acker, M.G., Antonakos, B., Chen, C.H.-T., Chen, Z., Cooke, V.G., et al. (2016). Allosteric inhibition of SHP2 phosphatase inhibits cancers driven by receptor tyrosine kinases. *Nature* **535**, 148–152.
- Cox, J., and Mann, M. (2008). MaxQuant enables high peptide identification rates, individualized p.p.b.-range mass accuracies and proteome-wide protein quantification. *Nat. Biotechnol.* **26**, 1367–1372.
- Cox, J., Hein, M.Y., Luber, C.A., Paron, I., Nagaraj, N., and Mann, M. (2014). Accurate proteome-wide label-free quantification by delayed normalization and maximal peptide ratio extraction, termed MaxLFQ. *Mol. Cell. Proteomics* **13**, 2513–2526.
- Cunnick, J.M., Mei, L., Doupnik, C.A., and Wu, J. (2001). Phosphotyrosines 627 and 659 of Gab1 constitute a bisphosphoryl tyrosine-based activation motif (BTAM) conferring binding and activation of SHP2. *J. Biol. Chem.* **276**, 24380–24387.
- Francavilla, C., Papetti, M., Rigbolt, K.T.G., Pedersen, A.-K., Sigurdsson, J.O., Cazzamali, G., Karemire, G., Blagoev, B., and Olsen, J.V. (2016). Multilayered proteomics reveals molecular switches dictating ligand-dependent EGFR trafficking. *Nat. Struct. Mol. Biol.* **23**, 608–618.
- Furdui, C.M., Lew, E.D., Schlessinger, J., and Anderson, K.S. (2006). Auto-phosphorylation of FGFR1 kinase is mediated by a sequential and precisely ordered reaction. *Mol. Cell* **21**, 711–717.
- Heldin, C.-H., and Lennartsson, J. (2013). Structural and functional properties of platelet-derived growth factor and stem cell factor receptors. *Cold Spring Harb. Perspect. Biol.* **5**, a009100.
- Humphrey, S.J., Azimifar, S.B., and Mann, M. (2015). High-throughput phosphoproteomics reveals *in vivo* insulin signaling dynamics. *Nat. Biotechnol.* **33**, 990–995.
- Jersie-Christensen, R.R., Sultan, A., and Olsen, J.V. (2016). Simple and Reproducible Sample Preparation for Single-Shot Phosphoproteomics with High Sensitivity. *Methods Mol. Biol.* **1355**, 251–260.
- Kim, M.-S., Pinto, S.M., Getnet, D., Nirujogi, R.S., Manda, S.S., Chaerkady, R., Madugundu, A.K., Kelkar, D.S., Isserlin, R., Jain, S., et al. (2014). A draft map of the human proteome. *Nature* **509**, 575–581.
- Koytiger, G., Kaushansky, A., Gordus, A., Rush, J., Sorger, P.K., and MacBeath, G. (2013). Phosphotyrosine signaling proteins that drive oncogenesis tend to be highly interconnected. *Mol. Cell. Proteomics* **12**, 1204–1213.
- Lemmon, M.A., and Schlessinger, J. (2010). Cell signaling by receptor tyrosine kinases. *Cell* **141**, 1117–1134.
- Mañes, S., Mira, E., Gómez-Moutón, C., Zhao, Z.J., Lacalle, R.A., and Martínez-A, C. (1999). Concerted activity of tyrosine phosphatase SHP-2 and focal adhesion kinase in regulation of cell motility. *Mol. Cell. Biol.* **19**, 3125–3135.
- Maroun, C.R., Naujokas, M.A., and Park, M. (2003). Membrane targeting of Grb2-associated binder-1 (Gab1) scaffolding protein through Src myristylation sequence substitutes for Gab1 pleckstrin homology domain and switches an epidermal growth factor response to an invasive morphogenic program. *Mol. Biol. Cell* **14**, 1691–1708.
- Olsen, J.V., Blagoev, B., Gnad, F., Macek, B., Kumar, C., Mortensen, P., and Mann, M. (2006). Global, *in vivo*, and site-specific phosphorylation dynamics in signaling networks. *Cell* **127**, 635–648.
- Ong, S.E., Blagoev, B., Kratchmarova, I., Kristensen, D.B., Steen, H., Pandey, A., and Mann, M. (2002). Stable isotope labeling by amino acids in cell culture, SILAC, as a simple and accurate approach to expression proteomics. *Mol. Cell. Proteomics* **1**, 376–386.
- Poulsen, J.W., Madsen, C.T., Young, C., Poulsen, F.M., and Nielsen, M.L. (2013). Using guanidine-hydrochloride for fast and efficient protein digestion and single-step affinity-purification mass spectrometry. *J. Proteome Res.* **12**, 1020–1030.
- Sharma, K., D'Souza, R.C.J., Tyanova, S., Schaab, C., Wiśniewski, J.R., Cox, J., and Mann, M. (2014). Ultradeep human phosphoproteome reveals a distinct regulatory nature of Tyr and Ser/Thr-based signaling. *Cell Rep.* **8**, 1583–1594.
- Tomar, A., Lawson, C., Ghassemian, M., and Schlaepfer, D.D. (2012). Cortactin as a target for FAK in the regulation of focal adhesion dynamics. *PLoS ONE* **7**, e44041.
- Tyanova, S., Temu, T., Sinitcyn, P., Carlson, A., Hein, M.Y., Geiger, T., Mann, M., and Cox, J. (2016). The Perseus computational platform for comprehensive analysis of (prote)omics data. *Nat. Methods* **13**, 731–740.
- Ubersax, J.A., and Ferrell, J.E., Jr. (2007). Mechanisms of specificity in protein phosphorylation. *Nat. Rev. Mol. Cell Biol.* **8**, 530–541.

- Vizcaíno, J.A., Deutsch, E.W., Wang, R., Csordas, A., Reisinger, F., Ríos, D., Dianes, J.A., Sun, Z., Farrah, T., Bandeira, N., et al. (2014). ProteomeXchange provides globally coordinated proteomics data submission and dissemination. *Nat. Biotechnol.* 32, 223–226.
- Wang, Y., Yang, F., Gritsenko, M.A., Wang, Y., Clauss, T., Liu, T., Shen, Y., Monroe, M.E., Lopez-Ferrer, D., Reno, T., et al. (2011). Reversed-phase chromatography with multiple fraction concatenation strategy for proteome profiling of human MCF10A cells. *Proteomics* 11, 2019–2026.
- Yaffe, M.B. (2013). The scientific drunk and the lamppost: massive sequencing efforts in cancer discovery and treatment. *Sci. Signal.* 6, pe13.
- Zhang, J., Zhang, F., and Niu, R. (2015). Functions of Shp2 in cancer. *J. Cell. Mol. Med.* 19, 2075–2083.

**Supplemental Information**

**Large-Scale Phosphoproteomics Reveals  
Shp-2 Phosphatase-Dependent Regulators  
of Pdgf Receptor Signaling**

**Tanveer S. Batth, Moreno Papetti, Anamarija Pfeiffer, Maxim A.X. Tollenaere, Chiara Francavilla, and Jesper V. Olsen**

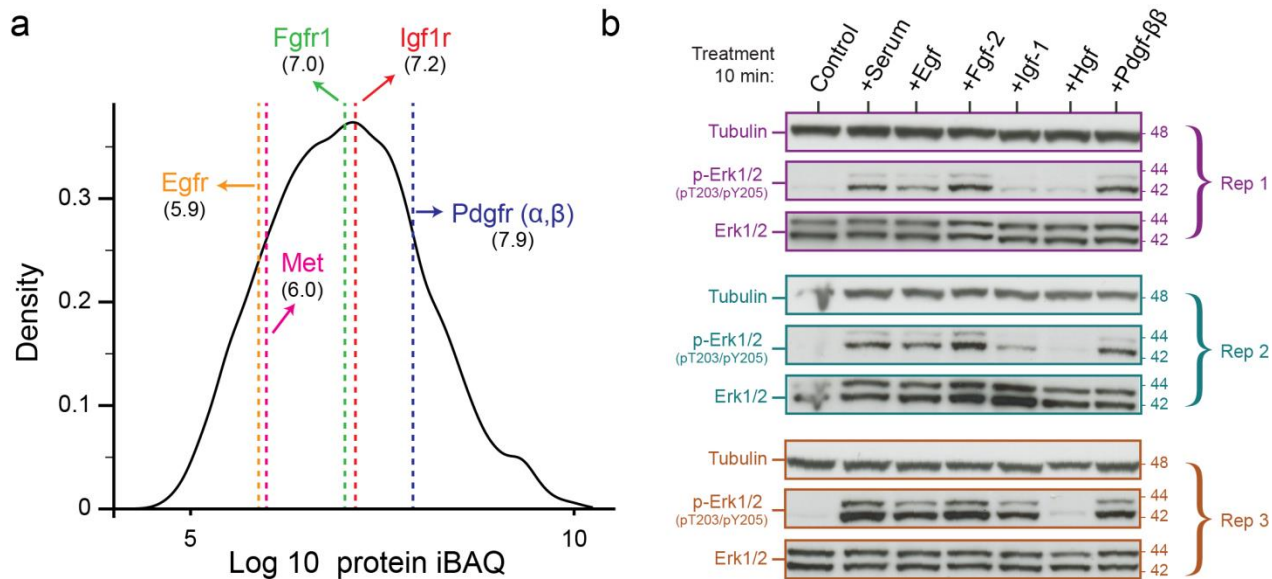


Figure S1. Relative abundance of RTKs and their respective ligand-induced phospho-Erk response, related to Figure 1.

(A) Density analysis of the relative protein abundance in unstimulated NIH/3T3 cells. RTKs abundance is highlighted and their respective log10 iBAQ values are shown. Pdgfr, Igf1r and Fgfr1 represent the most abundant RTKs. (B) Lysates from NIH/3T3 cells stimulated for 10 min with canonical ligands respective to their RTKs. The expression and activating phosphorylation of Erk1/2 were analyzed by immunoblotting in three independent biological replicates (Rep1, Rep2, and Rep3). Tubulin was used as loading control.

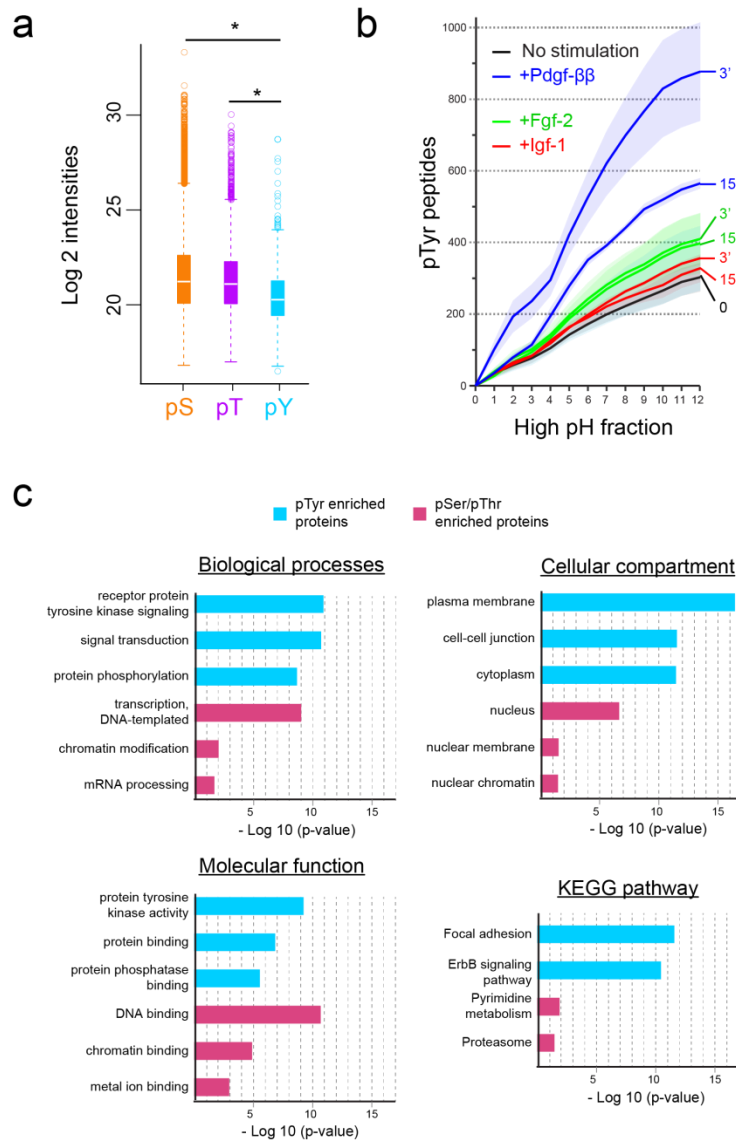


Figure S2. Analysis of phosphotyrosine peptides and pTyr containing proteins, related to Figure 1 and 2.

(A) Box plot of quantile normalized median intensity distributions of the different phosphorylation residues expressed on a log 2 scale. (B) Phosphotyrosine peptide variants accumulation over all the fractions for each of the indicated conditions is shown to highlight the strength of high pH reversed-phase fractionation step in our phosphoproteomics workflow. Values represent the mean  $\pm$  S.E.M. (shaded bars). (C) GO-term enrichment analysis comparison between phosphotyrosine- and phosphoserine/threonine-containing proteins. Analysis was performed based on all phosphoproteins across conditions that were identified in our dataset. \*, P < 2.2e-16.

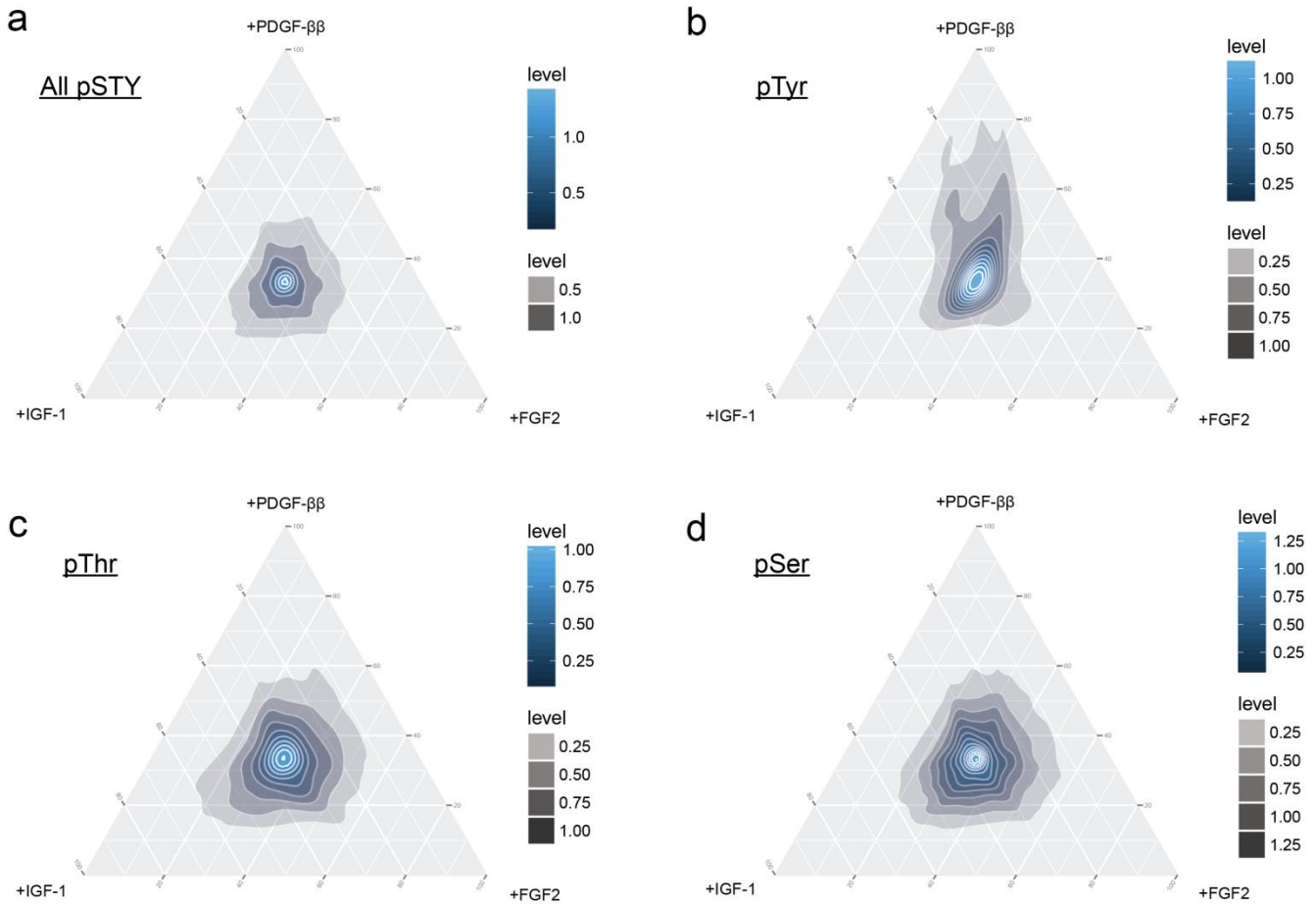


Figure S3. Density estimation of ligand-induced phosphorylation sites, related to Figure 2.

Kernel density estimation of phosphorylation sites upon differential ligand stimulation is shown in the ternary plot. Color bar represents distribution score and grey bar indicates opaqueness (A) Phosphorylation on serine, threonine and tyrosine residues were analyzed simultaneously (All pSTY). Individual density estimation of phosphorylation sites was performed for tyrosine (pTyr), threonine (pThr) and serine (pSer) (B, C, D).

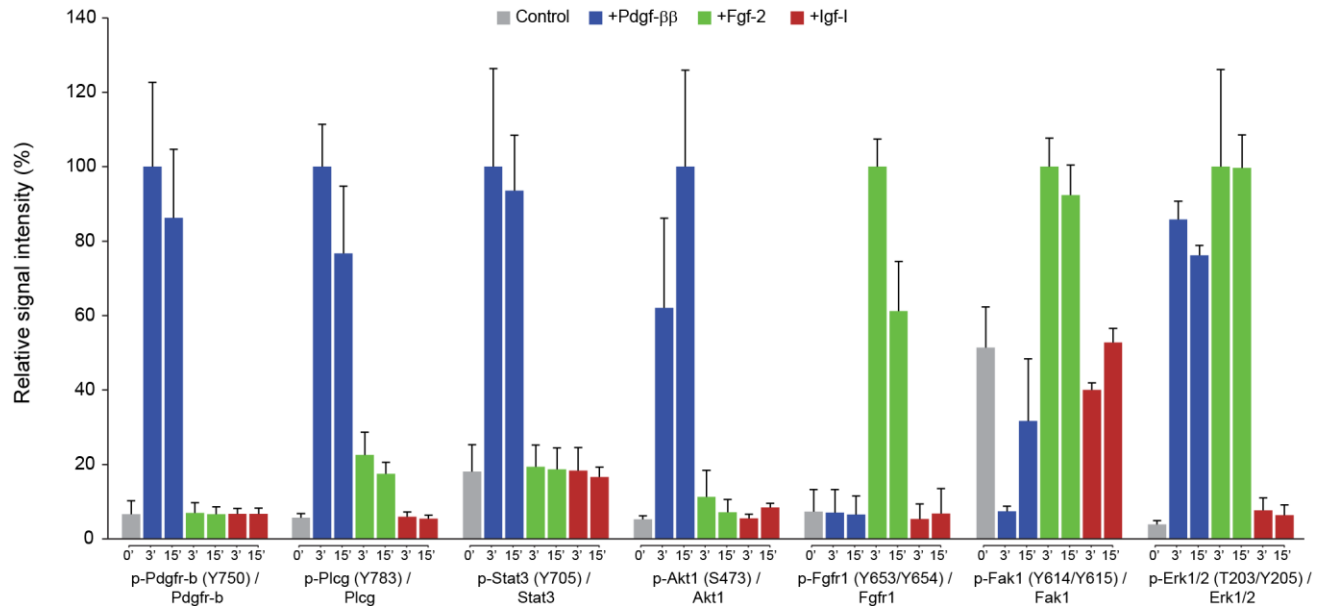


Figure S4. Western blot quantification of signaling pathways activation, related to Figure 3.

(A) The graph shows densitometric quantification of western blot bands for phosphorylated proteins at 3 and 15 minutes timepoint. Results validate the differential patterns of signaling pathways activation upon ligand stimulation observed in our phosphoproteomics dataset. Values are normalized to their total protein abundance and represented relative to the maximum phosphorylation signal from each condition. Data represent the means  $\pm$  S.E.M. of three independent experiments.

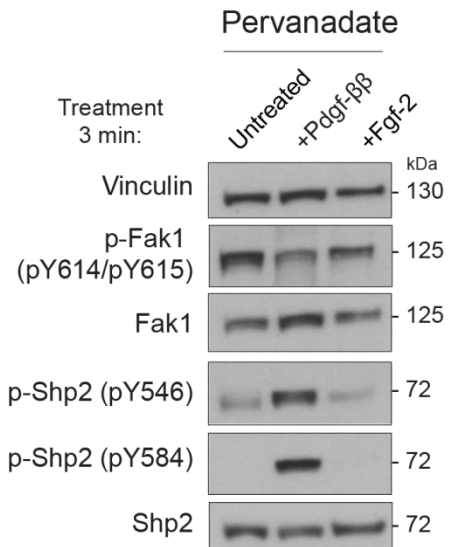


Figure S5. Protein tyrosine phosphatases affect Y614 and Y615 phosphorylation on Fak1, related to Figure 4.

(A) Lysates from pervanadate-treated cells and stimulated for 3 min with ligands were immunoblotted as indicated. Bands related to Fak1 phosphorylation are also shown after a longer exposure to emphasize the restored phosphorylation upon Pdgf- $\beta\beta$  stimulation. Vinculin was used as loading control.

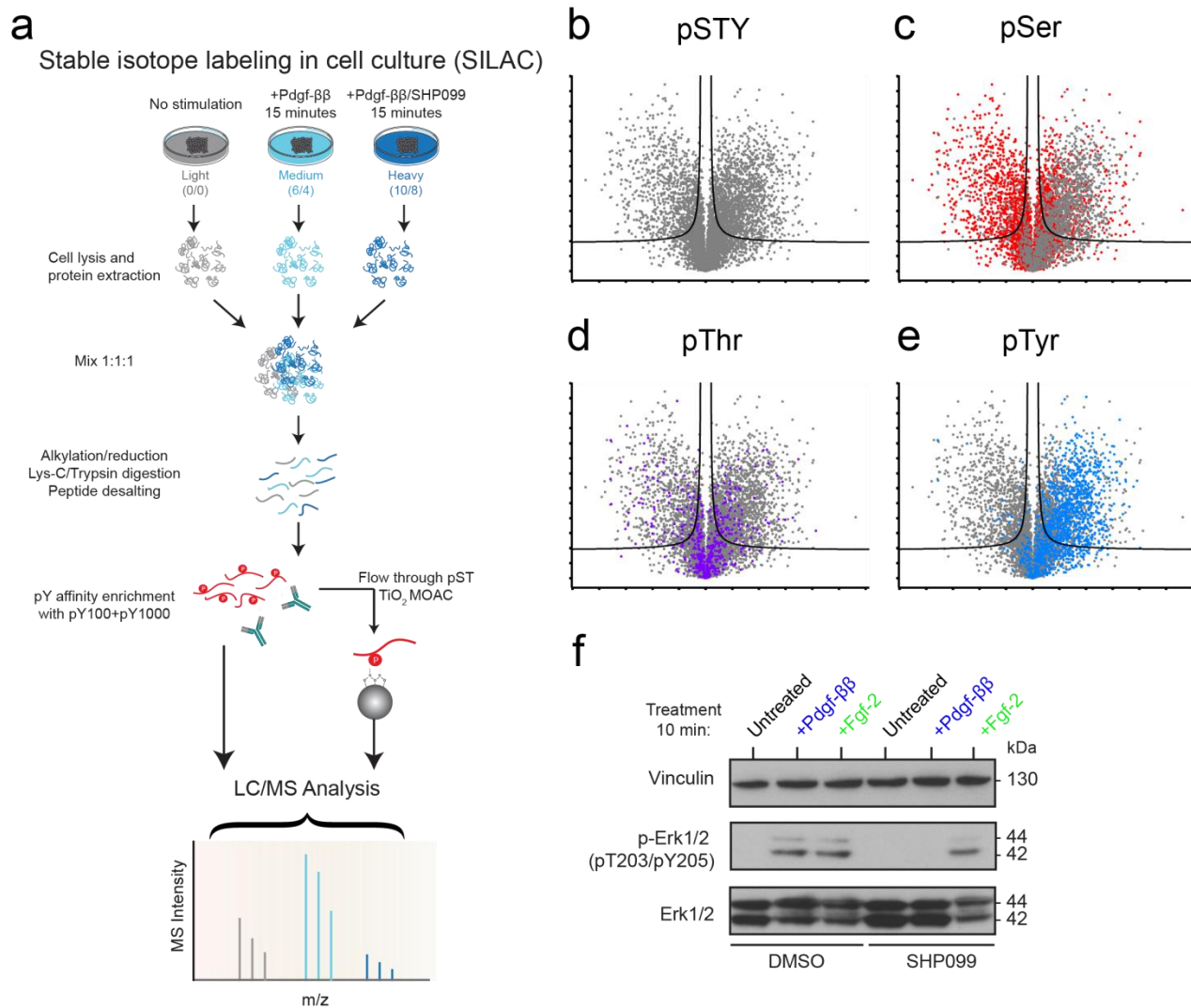


Figure S6. Phosphoproteomics SILAC analysis, related to Figure 5, Table S2, and experimental procedures.

(A) Experimental design and workflow for SILAC phosphoproteomics analysis. A triple SILAC design was utilized in which the different conditions were fixed at the protein level. After generation of Lys-C/Trypsin digestion, peptides were desalted and first enriched for phosphotyrosine (pTyr) containing peptides using antibodies. After enrichment of pTyr peptides, flow through was enriched for phosphoserine (pSer) and phosphothreonine (pThr) containing peptides using titanium dioxide and analyzed separately using LC/MS. See material and methods for details. (B-E) Volcano plots of SILAC phosphorylation site ratios (Medium/Light SILAC state vs Heavy/Light) comparing Pdgf- $\beta\beta$  stimulation with and without Shp2 inhibitor SHP099. Volcano plot was generated on Class I sites using with FDR of 0.05 and S0 at 0.1. (B) Volcano plot ratios in parallel of pTyr, pSer, and pThr (pSTY) shows global changes in the phosphoproteome with Shp2 inhibition. (C) pSer is highlighted in the global distribution of pSTY sites, similarly for (D) pThr, and (E) pTyr. (F) Western blot of phospho-Erk1/2 (Mapk) confirms the reduction in phosphorylation level of this activation site with Shp2 inhibition with Pdgf- $\beta\beta$  stimulation. However phospho-Erk activation is not abolished alongside Fgf-2 stimulation.

**a**

## Cortactin pY421

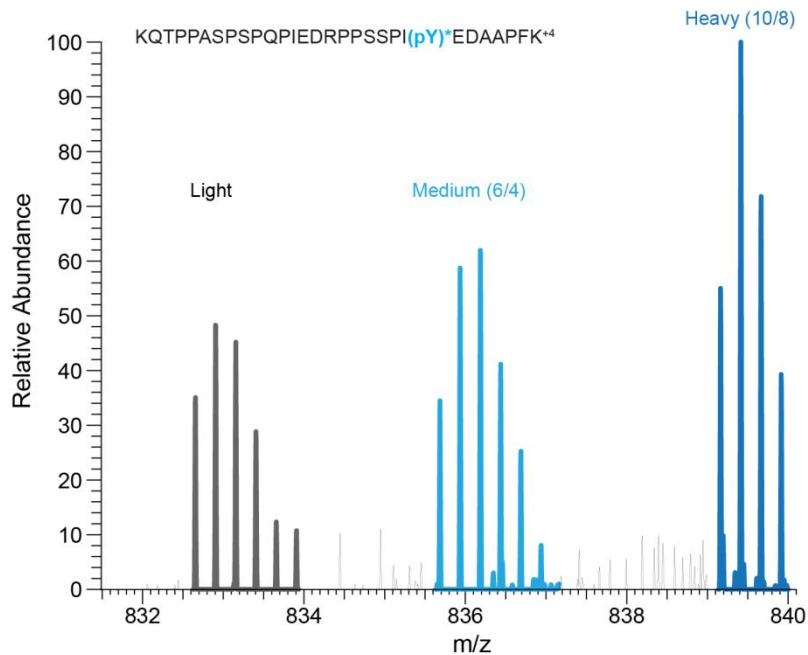
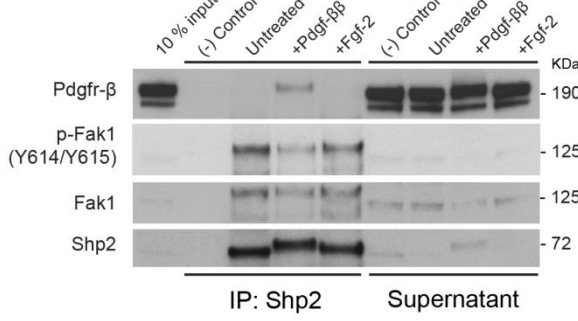
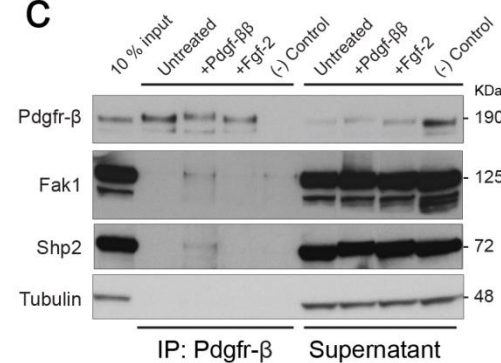
**b****c**

Figure S7. Cortactin phosphorylation at pY421 and recruitment of Pdgfr to Shp2/Fak1 complex, related to Figure 5.

(A) SILAC triplets extracted from .raw files are visualized to represent an increase in Cortactin pY421 with Shp2 inhibition and Pdgf-ββ stimulation from a tryptic peptide containing the phosphosite. Light (unstimulated) and medium (+Pdgf-ββ for 15 minutes) show relative similar levels of phosphorylation, however the phosphopeptide is upregulated in the heavy condition (+Pdgf-ββ w/SHP099 for 15 minutes) indicating upregulation of this specific site. (B) Lysates from cells stimulated with Pdgf-ββ and Fgf-2 for 3 minutes were immunoprecipitated for Shp2 (B) and Pdgfr-B (C). Following immunoprecipitation, samples were blotted with the indicated antibodies. Supernatant samples correspond to unbound fractions and were collected before the washing steps.